Chemical and Process Engineering: New Frontiers, 2025, 46(4), e114
DOI: 10.24425/cpe.2025.155552

Disperse Blue 1 as a multifunctional photosensitizer for enhanced photopolymerization kinetics and 3D printing of hydrogels

Dominika Krok-Janiszewska[1], Patryk Szymaszek[1], Paweł Niezgoda[1], Aneta Pietraszek[1], Joanna Ortyl[1,2,3*]

[1] Cracow University of Technology, Faculty of Chemical Engineering and Technology, Department of Biotechnology and Physical Chemistry, Warszawska 24, 30-155 Cracow, Poland
[2] Photo HiTech Ltd., Bobrzyńskiego 14, 30-348 Cracow, Poland
[3] Photo4Chem Ltd., Lea 114/416, 30-133 Cracow, Poland

* **Corresponding author, e-mail:** jortyl@pk.edu.pl

Article info:
Received: data1
Revised: data2
Accepted: data3

Abstract
Photopolymerization is a leading technology in coatings, adhesives, and additive manufacturing, where efficient photoinitiators are essential. This study highlights Disperse Blue 1, a commercially available organic dye, as a potent yet underexplored candidate for light-induced polymerization. Beyond its role as a colorant, Disperse Blue 1 exhibits remarkable photochemical reactivity, luminescence, and photostability. We investigate its function as both a photoinitiator and photosensitizer, demonstrating its capacity to initiate radical polymerization, enhance reaction kinetics, and synergize with iodonium salts in resin formulations for 3D printing. Its integration into 3D-VAT processes enables the fabrication of functional hydrogel structures, offering new opportunities in soft material design. These findings position Disperse Blue as a versatile component for next-generation photopolymer systems, supporting the development of tunable, high-performance materials for advanced manufacturing applications

Keywords
light, free-radical photopolymerization, hydrogel materials, 3D printing, Disperse Blue 1

1. INTRODUCTION

Light-induced processes are gaining popularity each year, expanding the spectrum of their potential applications to an increasing number of aspects of life and industry (Kamińska et al., 2015; Fiedor et al., 2020; Price et al., 2020; Tomal et al., 2021a). Photopolymerization is one of the processes of great interest (Fiedor et al., 2020; Topa, et al., 2020; Gibson et al., 2015; Tomal et al., 2021b). Owing to their flexibility, ease of modification of parameters, and wide possibilities of control, as well as observation and analysis of the process through the use of appropriate techniques, these processes have become an indispensable part of the additive technologies. They are thus fundamental for all derivatives and other applications that fully exploit additive technologies (Garino et al., 2021; Piedra-Cascón et al., 2021; Drury and Mooney, 2003; Hola et al., 2020; Nowak et al., 2018; Ortyl et al., 2013; Ortyl et al., 2012). Photopolymerization is an exoenergetic chemical process that occurs under the influence of light of a certain wavelength, the presence of which is the initiating factor of the process through the excitation of a photoinitiator. The presence of which is crucial in terms of electron transfer and the initiation of bond formation in the structure of the resulting polymer (Crivello and Reichmanis, 2014; Kabatc et al., 2017; Petko et al., 2022). The presence of a photoinitiator is often a limiting factor in the entire process (Bagheri and Jin, 2019). However, commercially available photoinitiators often absorb light in the short-wave range of approximately 300–320 nm (Le et al., 2021; Bao, 2022; Wierzbicki et al., 2021). Because of its high energy, this light is considered potentially dangerous to human vision; hence, the desire to make the whole process more accessible and safe for scientific use. This applies to the photopolymerization process itself, as well as to the SLA 3D printing that uses it, which has begun to undergo a transformation, starting to use light sources that emit lower energy at higher wavelengths (Lin et al., 2021; Petko et al., 2022). Currently, these values are approximately 405 nm, which provides the right balance that preserves the speed and efficiency of the process (Valeur and Berberan-Santos, 2012) while remaining safe for human vision (Al Rashid et al., 2021; Khadilkar et al., 2019). To change the absorption characteristics of the previously mentioned commercial photoinitiators, compounds with the ability to effectively absorb light at higher wavelengths and then transfer electrons to the photoinitiator structure for efficient process initiation (Hola et al., 2021; Le et al., 2021; Sun et al., 2023; Tomal et al., 2020) are gaining popularity. Their additional physicochemical properties, such as their ability to fluoresce or phosphoresce, further expand the possibilities of their application in additive 3D-VAT printing technologies by photosensitizing the radical photopolymerization process (Baryshnikov et al., 2017; Qu et al., 2012; Xiao et al., 2015).

The mechanism of the radical photopolymerization process is based on the generation of radicals by the photoinitiator, which in the active state leads to the addition of monomers, such as vinyl ethers (Bagheri and Jin, 2019; Decker et al., 2001; Peer et al., 2019). Owing to its high affinity for oxygen and oxygen inhibition during the process, the process must proceed more efficiently under special conditions, which in turn makes its implementation more difficult in terms of application and utility (Jasinski et al., 2018; Tasdelen et al., 2020). The biological activity or biocompatibility, as well as the lack of demonstrated cytotoxicity of the tested compounds, also provide additional value (Williams, 2008; do Nascimento et al., 2010). In addition, the possibility of using them in the form of photocurable hydrogel materials provides great opportunities in terms of biochemical use of the mentioned structures and combining the capabilities of both processes (Tomal at al., 2020; Chimene et al., 2016; You et al., 2019; Li et al., 2020). Hydrogel materials are polymers with properties that allow them to retain significant amounts of water in their structures while remaining solid (Ma et al., 2016). Structurally, they are hydrophilic polymer networks, which, owing to their flexibility and biocompatibility, find a spectrum of applications in fields such as the medical industry, pharmaceuticals, and tissue engineering (Liu et al., 2021; Tran et al., 2015; Distler and Boccaccini, 2020). These capabilities are guaranteed primarily by their ability to control the release of adsorbed active substances from inside the structure to the outside, which makes them highly desirable drug carriers or wound dressings (Larush et al., 2017; Tsegay et al., 2022).

The possibility of local drug release relieves the patient from constantly thinking about the next doses necessary to take in order to maintain the appropriate concentration of active substances in the body (Anselmo and Mitragotri, 2014). Moreover, in the case of dressings, the uniform and continuous release of active substances means that such a dressing will last longer without the need to constantly change it to a new one, which may be an extremely important aspect for potential consumers when choosing a solution for themselves (Kasprzyk et al., 2018). Hydrogel materials also find their way into the agricultural industry, where once again their hydrophilic nature is exploited (Dissanayake et al., 2024; Kalossaka et al., 2021; Schmidt, 2019). They are able to retain water in the soil, which prevents plants from drying out and helps ensure optimal conditions for growth, even under adverse weather conditions and periods of prolonged drought (El-Rehim et al., 2004). An extremely important aspect of shedding a huge amount of light on the possibilities of the structures under study is the current trend of green chemistry, which significantly influences the challenges and limitations faced by scientists around the world (El-Rehim et al., 2004; Sanchez-Rexach et al., 2020). The desire to reduce costs while maintaining process efficiency causes those involved in photochemical processes to search for new possible compounds, including those of commercial or plant origin (Fertier et al., 2013; Tehfe et al., 2013). The present work focuses on the use of a dye with the trade name 'Disperse Blue 1' (DB1) (Gulrajani, 2011). Full spectroscopic characterization was carried out starting from absorption and fluorescence properties, through a full spectrum of photostability studies of the structure under different conditions and under illumination with light of different wavelengths in the visible and near-infrared light range (Fiedor, et al., 2020; Tomal et al., 2020; Bao, 2022). Subsequently, the electrochemical characteristics of the oxidation and reduction potentials were also investigated to illustrate the potential of using the studied compound as a photosensitizer of photoinitiators in

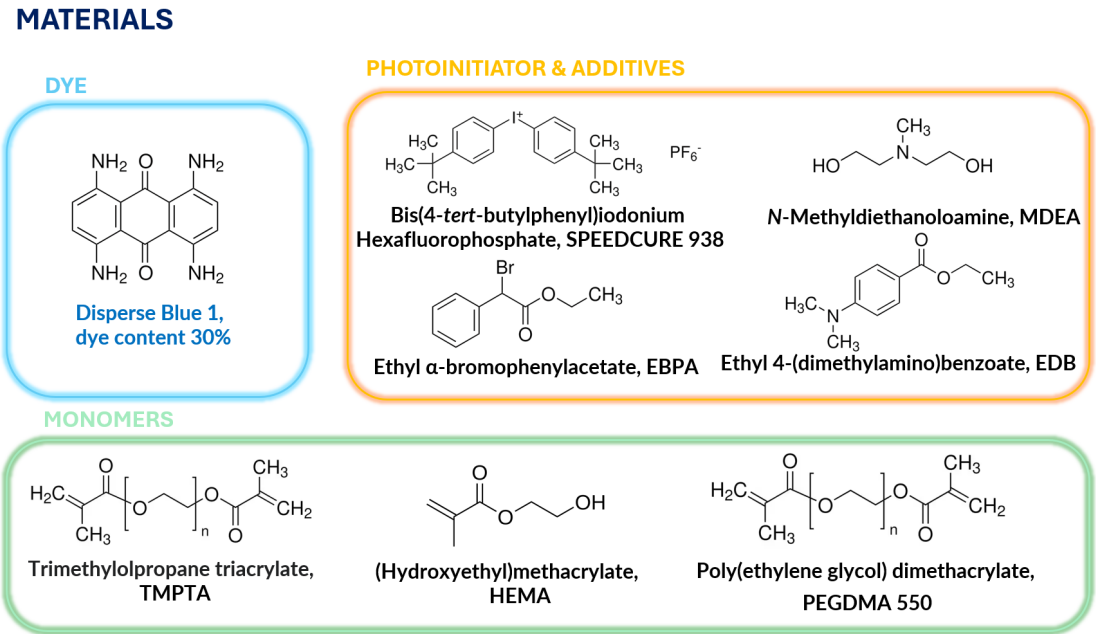

Figure 1. Dye, photoinitiators, additives and monomers used in paper.

the radical photopolymerization process by Real-Time FT-IR spectroscopy, and in subsequent steps in the process of additive formation of spatial objects (Currens et al., 2022; Hola et al., 2021; Tomal et al., 2021b; Scott et al., 2003). The studied compound, due to its neutral properties, fits perfectly into some aspects of green chemistry and the prevailing trend of using photosensitive processes to obtain spatial objects and has great potential for implementation in biological applications (Hola et al., 2020; Le et al., 2021; Ortyl et al., 2019; Petko et al., 2021; Hou et al., 2015; Williams, 2008).

2. MATERIALS AND METHODS

2.1. Materials

All reagents and solvents used in the synthesis were purchased from Sigma-Aldrich, Alfa Aesar, and AmBeed and used without further purification (Figure 1). The analytical-grade acetonitrile used for spectral measurements and photolysis was purchased from Fischer Chemicals. The following monomers were used to measure the photoactivity of the tested photoinitiators by infrared spectroscopy: trimethylolpropane diacrylate (TMPTA, Sigma Aldrich, Germany), (hydroxyethyl)methacrylate (HEMA, Sigma Aldrich, Germany), poly(ethylene glycol) dimethacrylate (PEGDMA550, Sigma Aldrich, Germany). Speedcure 938 was used as photoinitiator, while methyldiethanolamine (MDEA, Sigma Aldrich, Germany), eethyl α-bromophenylacetate (EBPA, AmBeed, Germany), and (EDB, Alfa Aesar, Germany) were used as other photoinitiating additives. The dye used for the study was 1,4,5,8-tetraaminoanthraquinone, (DB1, Sigma Aldrich, Germany).

2.2. Electrochemical properties

Voltammetric measurements were performed to determine the oxidation and reduction potentials of the studied compounds. For this purpose, an electrochemical analyzer M161 and an electrode stand M164 from MTM-ANKO, Poland, with a standard three-electrode cell were used. Voltammetry measurements were recorded at a scan rate of 100 mV s^{-1}. The working electrode was a glassy carbon electrode with a diameter of 3 mm (Mineral, Poland) and a platinum wire served as the auxiliary electrode. All the potentials were measured with respect to the Ag/AgCl (3M KCl) electrode, which was placed in a double bridge filled with a 3 M KCl solution in the upper part and a solution of the supporting electrolyte in a given solvent in the lower part. The two solutions were separated using a cotton wool plug and separated from the test solution using a thick ceramic frieze. The potential of this reference electrode at 25 °C was +0.209 V, relative to the standard hydrogen electrode (SHE). 0.1 M KCl in acetonitrile was used as the auxiliary electrolyte. All the measurements were performed in a dry argon atmosphere (5.0 Messer) at 25 °C.

2.3. Spectroscopic characterization

The absorption spectra of DB1 were analyzed using a SilverNova TEC-X2 spectrophotometer in the 190-1100 nm range. A deuterium-halogen UV/Vis light source (StellarNet, Inc., Tampa, FL, USA) was used in all the experiments in the 200–800 nm range. The fluorescence emission and excitation spectra of DB1 were analyzed using a FluoroMax-4P spectrofluorometer (Horiba, Kyoto, Japan). All spectra were recorded at varying excitation wavelengths ranging from 200 to 800 nm, using a slit width of 5 nm for both excitation and emission in each measurement. All measurements were performed in water at room temperature.

2.4. Real-time FT-IR photopolymerization experiments

The light-induced photopolymerization process was analyzed by real-time FT-IR using a FT-IR i10 NICOLET™infrared spectrometer with a horizontal adapter (Thermo Scientific, Waltham, MA, USA). The compositions analyzed in these experiments were prepared by dissolving appropriate amounts of the initiating system with various monomers under light-free conditions. The polymerization kinetics were studied using the FT-IR method via the observation of absorption peaks at specific wavelengths (corresponding to the functional group or bond of the monomers used). Hence, the conversion rate was calculated according to Eq. (1):

$$\text{Conversion}\,[\%] = \left(1 - \frac{\text{Area}_{\text{after}}}{\text{Area}_{\text{before}}}\right) x100\% \qquad (1)$$

where: $\text{Area}_{\text{before}}$ – the area of the absorbance peak corresponding to a given group or bond in the monomer before photopolymerization; $\text{Area}_{\text{after}}$ – the area of the same absorbance peak at a given polymerization time. The wavelengths corresponding to the groups or bonds during polymerization are presented separately for each monomer during the course of the investigation.

2.5. Initiating systems for radical photopolymerization of acrylate monomer TMPTA in UV light and methacrylate monomer PEGDMA 550 in VIS light

To study free radical photopolymerization, compositions consisting of TMPTA together with a binary and ternary initiator system were prepared: Speedcure 938 (1% wt.) as photoinitiator and Blue (0.1% wt.) as photosensitizer were prepared. EDB amine (1.5% wt.) was used as co-initiator. A few drops of the test composition were applied between the laminates and placed on a horizontal holder in the FT-IR spectrometer. The double bond was monitored continuously at approximately 6.143 cm^{-1} for 600 s. TMPTA monomer with 1% wt. iodonium salt was used as a reference. In addition, the composition

of EBPA (1% wt.) and Blue (0.1% wt.) as two-component photoinitiating systems and three-component systems of EBPA (1% wt.), EDB(1.5% wt.) and Blue (0.1% wt.) in the presence of TMPTA initiator were tested between the laminate fragments. Reference compositions without the addition of the blue dye were also measured. Subsequent studies were conducted on compositions with systems that initiate free-radical photopolymerization of the methacrylate monomer PEGDMA 550 under visible light. The initiation efficiency of various two- and three-component initiation systems consisting of Blue (0.1% wt.) with EBPA (1% wt.), EDB (1.5% wt.) and MDEA amine (1.5% wt.) composition with the methacrylate monomer under visible light was investigated.

2.6. DB1 based systems for radical photopolymerization of air-resistant polymer hydrogels

Free radical photopolymerization of PEGDMA 550/HEMA monomers in ratios of 1:1 and 8:2 was carried out to produce hydrogel materials. First, photocurable compositions consisting of Blue (0.1% wt.), Speedcure 938 (1% wt.) and MDEA amine (1.5% wt.), and a mixture of PEGDMA 550 monomer and HEMA in ratios of 1:1 wt. and also 8:2 wt. were prepared. The compositions were then applied to a 1.0 mm thick adapter. The photopolymerization process was carried out under UV-LED 405 nm, 505 nm, 530 nm, 565 nm, 590 nm, and 660 nm. The double-bond conversion was tracked using an FT-IR spectrometer at approximately 6.125 cm^{-1}.

2.7. Photo-rheology measurements

Photoreological tests were carried out using an Anton Paar rheometer (Physica MCR 302) equipped with a UV light-curing system and a 20 mm parallel plate geometry. A 405 nm LED was used as the light source, with the light output set at 6.5 [$mW \cdot cm^{-2}$] at the sample surface. Light intensity was measured using a PM160 – Si Sensor Power Meter (Thorlabs Inc., Tampa, FL, USA). In the experiment, the distance between the two plates was set to 0.1 mm, at a fixed frequency of 1 Hz and a distortion amplitude of 1%. To stabilize the system, the light was switched on 10 s after the start of the measurement.

2.8. Development of hydrogel polymer materials

A composition consisting of a three-component initiator system (Blue, Speedcure 938 and MDEA) in the presence of PEGDMA 550/HEMA 8/2 wt. monomers was used to obtain the hydrogel materials. This choice was justified by the fact that compositions with a higher proportion of PEGDMA 550 monomer showed better initiator properties during the radical photopolymerization tests. Using filament printing, three types of molds with a size of 1x1mm and different thicknesses of 1 mm, 1.5 mm and 2 mm were obtained. The hydrogels were cast and cured under visible light. The dimensions of the materials were determined immediately after curing and after 12h and 48h of incubation in water.

2.9. Three-dimensional printing of the hydrogel model structure

3D-VAT printouts were obtained using a Lumen X+TM printer (Cellnk Inc., USA, supplied by Sygnis SA, Poland), which is a specialized polymer printer equipped with a light-emitting projector with a wavelength of 405 nm. It is an additive process; a laser printer (DK-8-KZ, NEW) equipped with a laser light source at 405 nm (spot diameter: 50 μm) was also used to produce 3D models. All 3D printouts obtained were analyzed on a DSX1000 digital microscope with a DSX10-SXLOB3X objective at a magnification of 42-420X.

2.10. Source of light

The light sources used for the real-time FTIR experiment were 405 nm, 505 nm, 530 nm, 565 nm, 590 nm, and 660 nm. The LED was powered using a DC2200 driver (Thorlabs, Tampa, FL, USA). The distance between the radiation source and the sample was 210 mm.

3. RESULTS

3.1. Determination of the spectroscopic properties of DB1

The UV-visible absorption spectrum of DB1, shown in Fig. 2, displays two major absorption bands. The first band at $\sim$ 300 nm (ultraviolet region) and the second overlapping band (600 nm region-visible region) were due to electronic transitions within the conjugated structure of the molecule. The absorption in the UV region is due to $\pi \rightarrow \pi^*$ transitions. These transitions were due to the presence of an aromatic ring system in the anthraquinone chromophore. Owing to its extended π-electron system, the anthraquinone structure enables strong absorption in this region. The presence of -NH2 electron-donating groups attached to the aromatic system intensified the band by enhancing the charge distribution and stabilizing the excited states. Sizeable visible absorption indicates the presence of $n - \pi$ transitions. The lone pairs on the oxygen atoms of the anthraquinone carbonyl (C=O) groups caused such transitions. Furthermore, substituents containing an amino group ($–NH_2$) can shift this band toward longer wavelengths (bathochromic shift) because of the resonance and inductive influence of electron-donating substituents. The delocalization of π-electrons is extended because of this interaction, lowering the energy gap between the ground and excited states (Table 1).

Table 1. Summary of spectroscopic parameters

Acronym/ Wavelength	λ_{max-ab} [nm]	ε_{238}	ε_{365}	ε_{405}	ε_{470}	ε_{505}	ε_{530}	ε_{565}	ε_{595}	ε_{660}
		[dm^3· mol^{-1}· cm^{-1}]								
DB1	238	8682	180	54	113	775	1443	2720	3783	1631

For spectroscopic studies, the concentration of disperse was in the range: 5.7×10^{-5} mol dm^{-3}

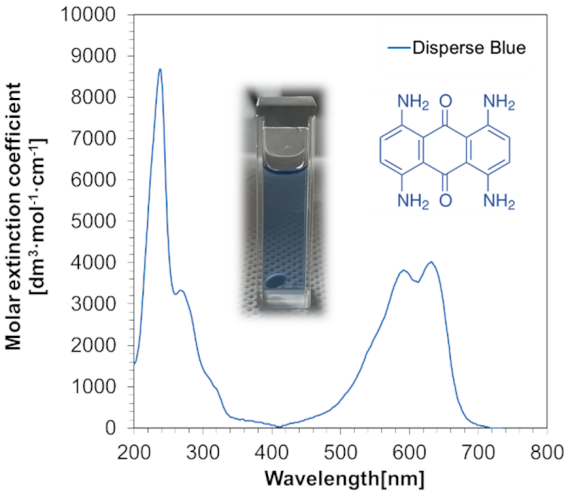

Figure 2. UV–visible absorption spectra of the examined DB1.

DB1 is a good candidate for being a photosensitizer because of its absorption in the visible region. Photosensitizers require light-enhanced reactions. They absorb light and transfer energy. DB1 possesses the following attributes that help its photosensitizing: 1) long chain conjugation, which helps in the effective absorption of light and transfer of energy; 2) bathochromic shift, which helps in the absorption of the visible spectrum where the abundance of light sources such as the sun are present; 3) amino groups modify absorption and may intervene in redox processes, thus enhancing reactivity.

HOMO and LUMO orbitals of DB1 explain its electronic structure. Thus, the HOMO level of DB1 is –4.70 eV. It is mainly localized over the aromatic system with a large degree of conjugation, which is responsible for $\pi \rightarrow \pi^*$ transitions. The anthraquinone core also delocalizes the LUMO with an energy of -2.39 eV, offering a complementary electronic distribution for $n \rightarrow \pi^*$ transitions. The HOMO-LUMO gap is sufficiently small for the molecule to absorb visible light, as shown in the UV-visible spectrum. The correct placement of the HOMO and LUMO causes a large spatial overlap of the orbitals. This overlap can aid in electronic transitions such as charge transfer (CT) and energy/electron transfer processes.

3.2. Photochemical behaviour of DB1

DB1 was examined under light conditions that can serve as a photosensitizer. Other types of diodes were also used in addition to typical UV light irradiation. In the first trial, the dye was irradiated in acetonitrile (ACN) at different monochromatic wavelengths (405, 430, 455, 505, 530, 565, 595, and 660 nm). The absorbance spectra exhibited different peaks corresponding to the features of the dye. Irritation of the sample resulted in a decrease of absorbance over time, especially for the shorter wavelengths of 405 nm and 455 nm, indicating the photodegradation of the dye. The extent of this deterioration was quantified at different wavelengths: the higher the photon energy present at shorter wavelengths, the greater the changes. The above observations indicate that the end of the absorbance range with shorter wavelengths can excite the dye effectively, thus making it more competent at initiating photochemical reactions. This is an important characteristic that needs to be evaluated when considering the compatibility of dyes as photosensitizers.

Ethyl 4-(dimethylamino)benzoate (EDB) was added to the dye solution at 8.62×10^{-3} mol/dm^3. The monitored absorbance reductions in this system were less pronounced than those for the dye alone. In addition, the spectral shifts detected were in the 650-750 nm range, which suggests electron transfer or stabilization effects. The EDB results either quenched or donated an electron, reducing the limit of photodegradation and enabling photosensitization. This dual behavior is useful in applications where photostability is required. Similar experiments used methyl diethanolamine (MDEA), at 13.9×10^{-3} mol/dm^3 concentration. The absorbance changes in the MDEA system were not as dramatic as those in the EDB system, with only slight changes occurring at 400-450 nm. MDEA may also act as an electron donor, with weaker stabilization effects than those of EDBs. The results indicate that the co-sensitizers EDB and MDEA can affect the photostability of the dye and offer an opportunity for the design of photosystems.

Following experiments made with a Speedcure 938 concentration of 3.09×10^{-3} mol/dm^3, the absorption spectra showed a substantial shift and peak broadening, especially in the visible region (500–600 nm). A significant change was observed after irradiation. The change in the spectrum shows that Speedcure 938 and the dye interact strongly, which can enhance the photosensitizing efficiency of the dye. The interaction of the dye with Speedcure 938 shows that the mixture can easily absorb and exhibit activity in visible light (Fig. 3).

A comparison of the results across all systems revealed that the photostability of DB1 was highest in the presence of EDB and MDEA. At the same time, the dye alone exhibited the most pronounced photodegradation. However, the addition

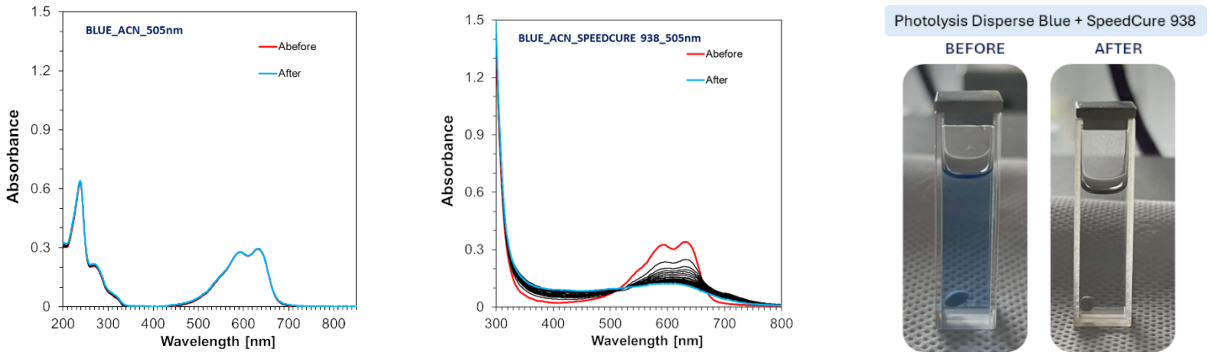

(a) (b)

Figure 3. (a) Photolysis of DB1 in acetonitryle (b) Photolysis of DB1 with Speedcure 938 in acetonitrile.

of Speedcure 938 enhanced the absorption of the dye in the visible region, indicating its potential for improving the overall photosensitization efficiency. These results demonstrate that the photophysical properties and stability of dyes can be modulated by adding specific co-sensitizers or additives, enabling tailored applications in photopolymerization. The wavelength dependence of photodegradation underscores the importance of selecting appropriate irradiation sources to optimize the photochemical performance of the dye.

3.3. Real-time FT-IR experiments

3.3.1. Free-radical photopolymerization of acrylate monomer

Photopolymerization with free radicals is the most popular process for obtaining polymeric materials because of the large number of monomers capable of undergoing polymerization. Other advantages are the high Speedcure 938 level of photopolymerization or control, which can be adopted for the kinetics. The majority of the monomers used in this process are acrylate- and methacrylate-based. However, acrylates are more frequently employed and are the more active monomers devoted to light-induced polymerization. In current applications of the polymerization process, the light sources most often emit out of the safe, visible range at 405 nm, which is their key. Consequently, a light-emitting diode with a wavelength of 405 nm was used for further investigations.

The FT-IR results, which help to study photopolymerization, lead to a different conclusion under different conditions. The conclusion is based on a specific photoinitiator system and co-initiators. The selection of the components (oxidizing agent, photoinitiator, and co-initiator) is represented by the conversion curves. These choices greatly influence the polymerization rate and conversion.

The system displayed three different behaviors with iodonium salt used as an oxidation agent. The system containing only EDB as the co-initiator (blue/EDB/TMPTA) polymerized the slowest, with the final conversion not exceeding 15% (Fig. 4). This means that while the oxidative cycle can generate radicals, it will not be able to polymerize materials effectively without other synergistic effects. With the Speedcure 938 photoinitiator (Blue/Speedcure 938/TMPTA), the conversion improved to approximately 30% and the polymerization rate was slow. Speedcure 938 is more reactive and easily forms radicals via the oxidative cycle. However, the best system using Speedcure 938 with EDB (Blue/Speedcure 938/EDB/TMPTA) recorded conversion above 50%. The synergy between the oxidation and reduction cycles of this formulation enhances radical generation and curing.

Similar trends were observed in the system employing bromide as the oxidizing agent, although the overall efficiency was lower than that of iodonium-based systems. The two-component system DB1/EBPA/TMPTA showed moderate conversion ($\sim$ 15%), while DB1/EDB/TMPTA exhibited a slightly higher conversion ($\sim$ 20%), indicating comparable efficiencies for these two-component systems. The highest conversion was achieved with the three-component DB1/EBPA/EDB/TMPTA system, highlighting the synergistic effect of the oxidative-reductive cycle involving all three components (Fig. 5).

Mechanistic schemes provide a better understanding of the observed trends. In an iodonium-based system, the salt is a reactive oxidizing agent that generates PhI^+ cations that drive the oxidation cycle. EDB is a key player in the reductive process, which donates electrons to regenerate the active photoinitiator species (BLUE*) for continuous radical production. The Speedcure 938/EDB system shows exceptional performance owing to this dual-cycle system, which works simultaneously. In contrast, the bromide-based system initiates the oxidative cycle by forming R+ and Br radicals through the action of bromide ions. Although it is less reactive than iodonium salts, bromide is a useful initiator of polymerization. The reduction cycle of EDB was enhanced, whereas the addition of EBPA increased the electron-donating capacity and enhanced the performance.

These findings show how valuable it can be for the co-initiation of photoinitiators. The polymerization rate and conversion greatly increased when a mixture of Speedcure 938 and EDB, EDB, and EBPA was used because both pathways were acti-

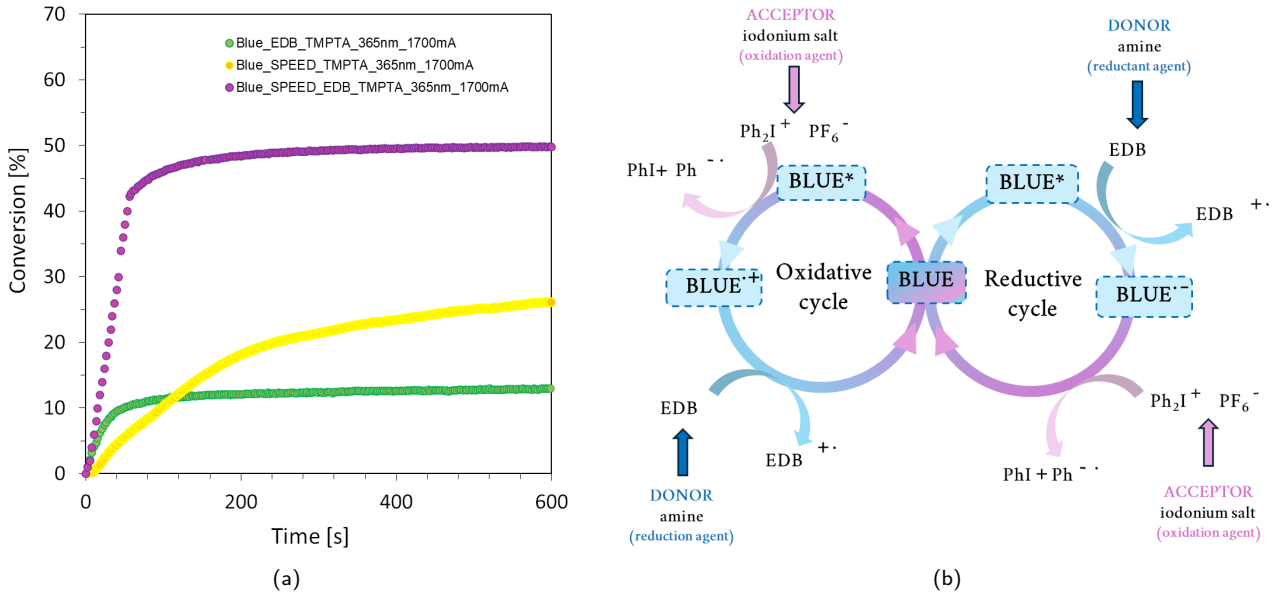

(a) (b)

Figure 4. (a) Radical photopolymerization profiles (acrylate function conversion *vs.* irradiation time) initiated by a bimolecular photoinitiating systems based on DB1 (0.1% wt.), IOD (1% wt.) and EDB (1.5% wt.) under irradiation at 365 nm. (b) A catalytic cycle using the DB1 under study.

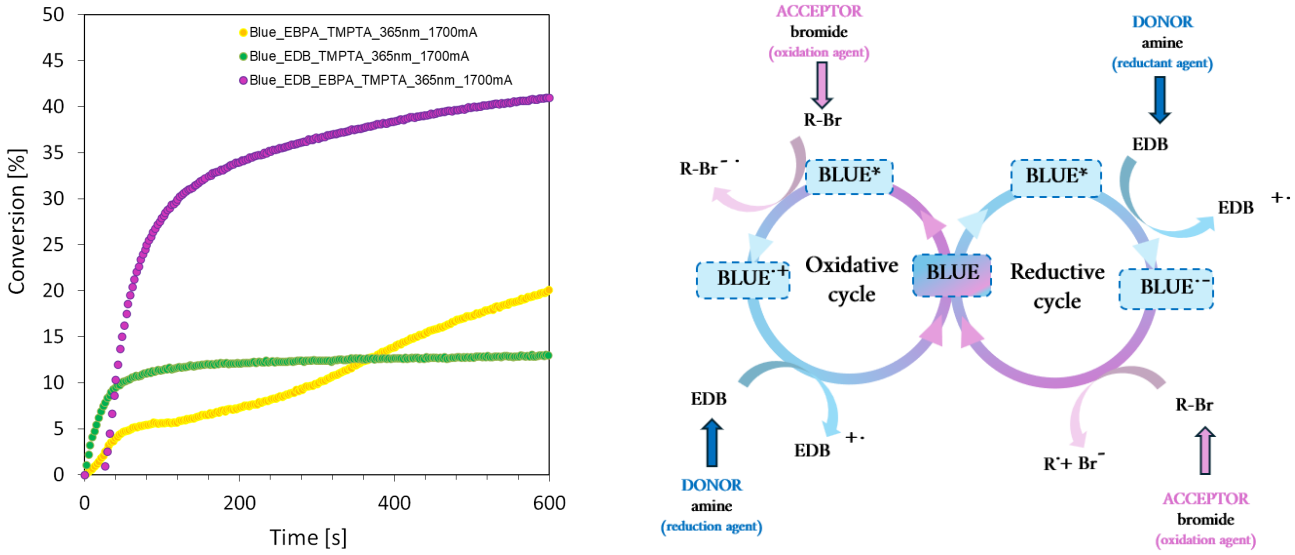

(a) (b)

Figure 5. (a) Radical photopolymerization profiles (acrylate function conversion *vs.* irradiation time) initiated by a bimolecular photoinitiating systems based on DB1 (0.1% wt.), EBPA(1% wt.) and EDB (1.5% wt.) under irradiation at 365 nm. (b) A catalytic cycle using the DB1 under study.

vated. In addition, the choice of oxidizing agent is important, as iodonium salts are more reactive than bromide. The results of the above investigation have identified the need for efficient and rapid photopolymerization and its advanced utilization in photopolymer science.

To complement the photopolymerization studies, the developed initiating systems with PEGDMA 550 monomer were also tested. The results presented in Fig. 6 show that, depending on the radiation length used, different degrees of monomer conversion were obtained. Moreover, ternary systems with blue dyes have the best application potential, and the highest conversion rates have been achieved. Experiments were also carried out for binary and ternary systems in the presence of the Speedcure 938 initiator, EDB amine, and blue dye in the PEGDMA 550 monomer. The results are shown in Fig. 7. The obtained conversion rates of methacrylate monomer indicate that, as described above, ternary systems are the best for initiating radical photopolymerization.

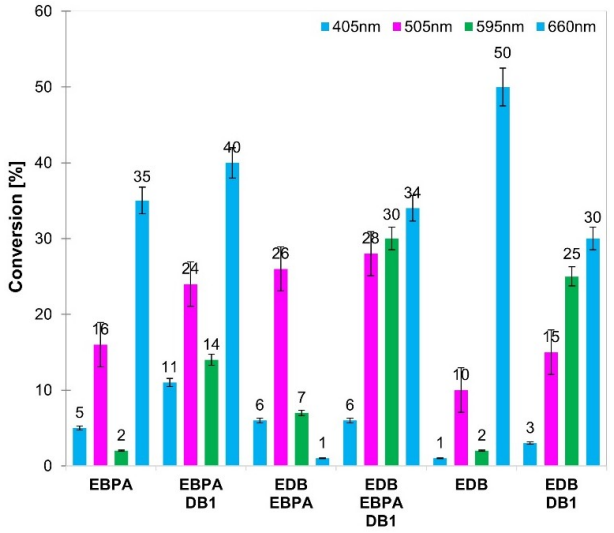

Figure 6. Radical photopolymerization profiles (acrylate function conversion *vs.* irradiation time) initiated by photoinitiating systems based on DB1 (0.1% wt.), EBPA(1% wt.) and EDB(1.5% wt.) with monomer PEGDMA 550 in laminate conditions. Irradiated at different wavelengths @405 nm, @505 nm, @595 nm and @660 nm.

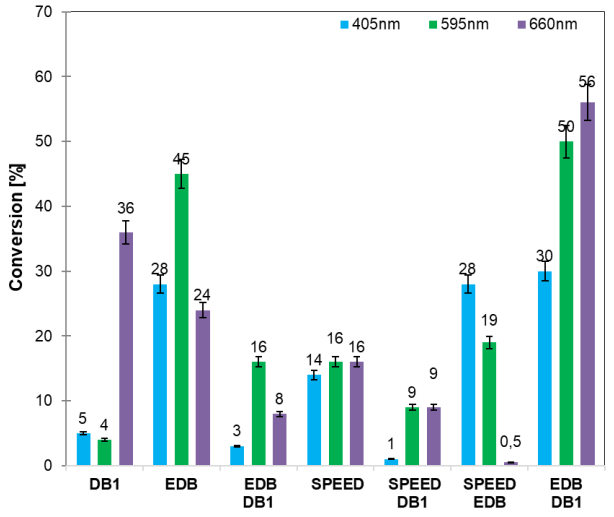

Figure 7. Radical photopolymerization profiles (conversion of acrylate function as a function of exposure time) initiated by photoinitiating systems based on DB1 (0.1% wt.), Speedcure 938 (1% wt.) and EDB (1.5% wt.) with PEGDMA 550 monomer under laminate conditions. Irradiated at different wavelengths @405 nm, @595 nm and @660 nm.

The actions of MDEA amine were also analyzed to compare its effects on systems composed of iodonium salt and Blue dye. It turned out that such systems performed better than previously described. This therefore prompted further research on the developed systems and on applications in 3D printing.

The obtained conversion rates of binary systems are not very high. However, in the iodonium salt-MDEA-dye Blue system, conversion rates as high as 50% were obtained upon irradiation with a wavelength of 660nm (Fig. 8). From the point of view of application in 3D printing, the wavelength of interest is 405 nm. At this wavelength, the developed initiator systems showed slightly lower conversion rates. However, they were still satisfactory and prompted further research.

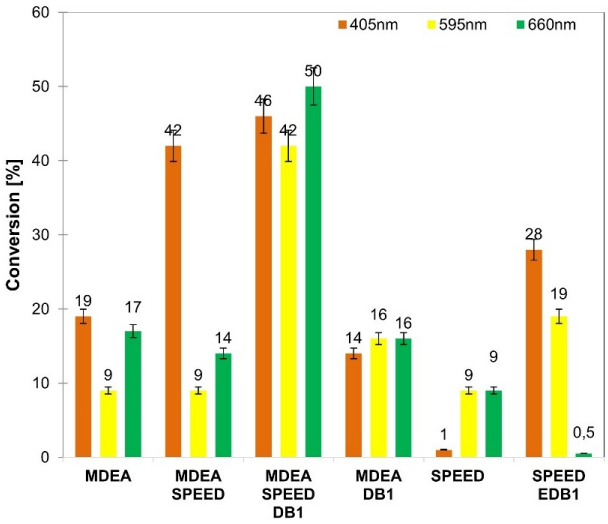

Figure 8. Radical photopolymerization profiles (conversion of acrylate function as a function of exposure time) initiated by photoinitiating systems based on DB1 (0.1% wt.), Speedcure 938 (1% wt.) and MDEA (1.5% wt.) with PEGDMA 550 monomer under laminate conditions. Irradiated at different wavelengths @405 nm, @595 nm and @660 nm.

The FT-IR conversion data presented herein provide a complete overview of the photopolymerization efficiency at different wavelengths, photoinitiator systems, and co-initiators. The results show that the interaction between oxidative and reductive cycles is crucial for the polymerization rate and final conversion (Figs. 9, 10).

The polymerization process was the most efficient for all studied systems at 405 nm, corresponding to violet high-energy light. The photons at this energy effectively excited the photoinitiator and quickly formed radicals. The system containing PEGDMA 550, bromide, BLUE, and EDB exhibited the highest conversions (Table 2). This shows that the significance of EDB as a reductive co-initiator strengthens the regeneration of the active photoinitiator species and helps the bromide-driven oxidative cycle. On the other hand, systems without BLUE or EDB showed a much slower polymerization rate and conversion, demonstrating the need for synergy between both.

Because of the lower photon energy, the polymerization efficiency was lower at 505 nm than at 405 nm. Even so, the system containing PEGDMA 550, bromide, BLUE, and EDB exhibited the highest conversion, suggesting the important role of EDB in sustaining the formation of radicals through the reductive cycle. The systems that do not contain EDB or blue light show lower rates, suggesting that a single-cycle mechanism (oxidative or reductive) cannot maintain high efficiency at this intermediate wavelength.

Table 2. Values of conversion compositions consists of bimolecular photoinitiating systems based on Blue (0.1% wt.), Speedcure 938 (1% wt.) and MDEA (1.5% wt.) under irradiation at 365 nm, (a) PEGDMA 550:HEMA ratio 1:1 (b) PEGDMA 550:HEMA ratio 8:2.

	Initiating system	Monomers	Conversion (%) @405 nm	@505 nm	@530 nm	@565 nm	@595 nm	@660 nm
a)	Blue MDEA Speedcure 938	PEGDMA 550/HEMA 1/1	78	52	54	73	38	75
b)	Blue MDEA Speedcure 938	PEGDMA 550/HEMA 8/2	81	55	70	85	63	84

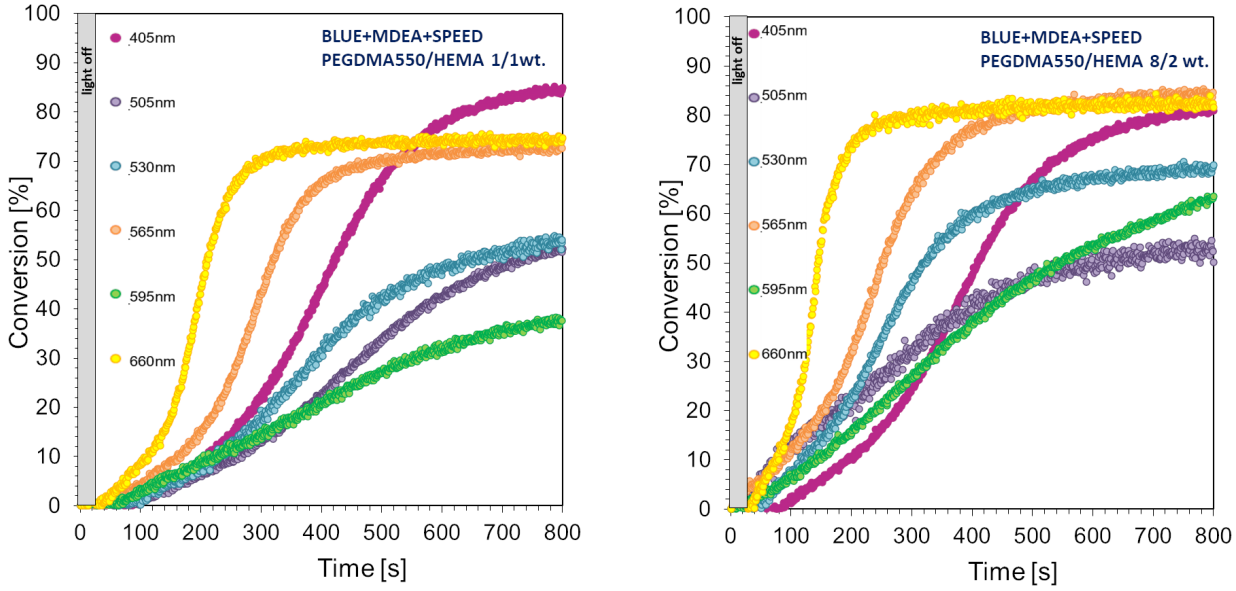

Figure 9. Radical photopolymerization profiles (acrylate function conversion *vs.* irradiation time) initiated by a bimolecular photoinitiating systems based on DB1 (0.1% wt.), Speedcure 938 (1% wt.) and MDEA (1.5% wt.) under irradiation at 365 nm, (a) PEGDMA 550:HEMA ratio 1:1 (b) PEGDMA 550:HEMA ratio 8:2, thickness of hydrogel 1 mm.

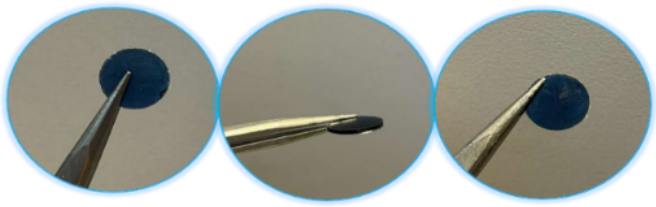

Figure 10. 2D gel material produced by radical photopolymerization of PEGDMA 550/HEMA 1/1 monomers in the presence of a ternary photoinitiator system based on Blue (0.1% wt.), Speedcure 938 (1% wt.) and MDEA (1.5% wt.), thickness of hydrogels 1 mm.

As the wavelength increases to 595 nm and 660 nm, which correspond to red and deep red light, respectively, the photopolymerization process increasingly relies on the reductive cycle. At these wavelengths, the lower photon energy diminishes the efficiency of the oxidative cycle, which explains the poor performance of bromide-based systems in the absence of extra co-initiators. Oppositely, the formulation with PEGDMA 550, BLUE, and EDB has the highest conversion levels, even above those with Br^-. These results show the vital importance of EDB, which effectively regenerates the active photoinitiator species in the reductive cycle to compensate for the lowered activity of the oxidative cycle at longer wavelengths.

When looking at the key performance indicators of photoinitiator systems, BLUE is important for achieving high polymerization efficiency. Systems containing BLUE always perform better than bromides or other co-initiators. Regarding shorter wavelengths such as 405 nm, Speedcure 938 benefits the oxidative cycle, making it a great performance enhancer. However, BLUE and EDB work best at all wavelength levels because EDB helps the reductive cycle and supports the ongoing formation of radicals, even at a lower energy wavelength.

These outcomes emphasize the use of co-initiators. As a reducing co-initiator, EDB enhances the efficiency of various polymerization and photopolymerization processes by ensuring the prolonged reopening of newly generated active photoinitiator species. Conversely, bromide mainly supported the oxidative cycle. It also performs well at higher-energy wavelengths. However, it cannot perform efficiently under red and deep red light. Speedcure 938 effectively participates in the oxidative cycle at short wavelengths (300–380 nm), assisting the action of BLUE and increasing the polymerization rate.

More energy is gained by the faster photon (405 nm) radiation, which helps in the polymerization process. In contrast, longer wavelengths (e.g., 595 nm and 660 nm) require the addition of reductive co-initiators, such as EDB, for high efficiency. The formulation containing PEGDMA 550, BLUE, and EDB is the most effective mixture, as it achieves high conversions at all wavelengths owing to an equal balance of oxidation and reduction. Our work stands out from previous studies on Disperse Blue 1, which have mainly focused on its dye role and light absorption characteristics or photocatalytic degradation processes (Saquib et al., 2008). We show for the first time that this commercially available dye can perform a dual function – an effective photoinitiator and photosensitizer – capable of initiating free radical polymerization and significantly accelerating its kinetics. Moreover, we demonstrate its synergistic effect with iodonium salts in resin formulations, which translates into high efficiency of 3D-VAT photopolymerization processes. Our research thus expands the applications of Disperse Blue 1 from a classical dye to a multifunctional component of modern photopolymer systems, enabling the fabrication of functional hydrogels and opening new perspectives in the design of soft materials for advanced 3D printing.

3.4. Photo-rheology

The results show how the monomer compositions photopolymerize under different wavelengths of light. These findings are discussed in detail below (Fig. 11, Table 3).

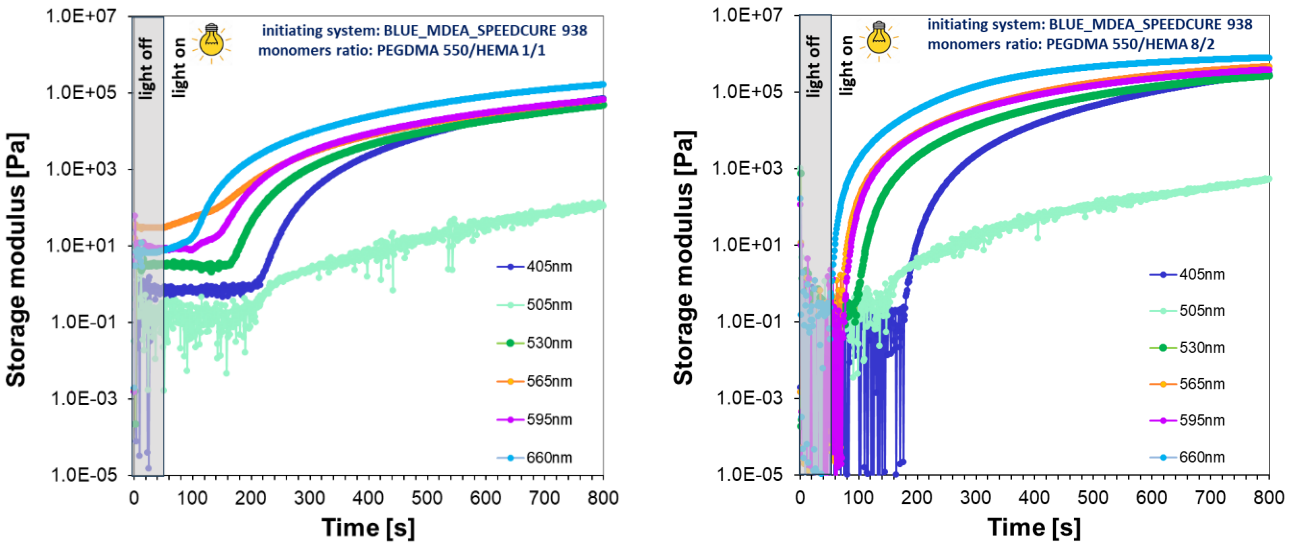

Figure 11. Storage modulus. G′ versus irradiation time of the photoinitiating systems based on Blue (0.1 wt%), Speedcure 938(1.0 wt.%) and MDEA (1.5 wt.%), film thickness 100 µm. (a) PEGDMA 550:HEMA ratio 1:1 wt. (b) PEGDMA 550:HEMA ratio 8:2 wt.

Table 3. Values of induction time compositions consists of bimolecular photoinitiating systems based on Blue (0.1% wt.), Speedcure 938(1% wt.) and MDEA (1.5% wt.) under irradiation at 365nm, (a) PEGDMA 550:HEMA ratio 1:1 wt. (b) PEGDMA 550:HEMA ratio 8:2 wt.

Initiating system	Monomers	Induction time (s)					
		@405 nm	@505 nm	@530 nm	@565 nm	@595 nm	@660 nm
Blue MDEA Speedcure 938	PEGDMA 550/HEMA 1/1 wt.	216	211	164	149	140	98
Blue MDEA Speedcure 938	PEGDMA 550/HEMA 8/2 wt.	178	159	93	75	77	55

Figures 12a and 12b show the effect of monomer composition and light wavelength on curing by plotting storage modulus (G') *vs.* time. The initial results, relating to the PEGDMA 550/HEMA system in a 1:1wt. ratio, give a substantial increment of the storage modulus by light activation in the 405–660 nm wavelength range. Photoirradiation of shorter wavelengths, namely 405 nm, shows the fastest growth and the highest final storage modulus values due to the more significant photoinitiation efficiency for high-energy wavelengths. The final modulus value at longer wavelengths (595 nm and 660 nm) is lower, and the curing is slower, indicating lesser photoinitiation efficiency.

The results for the PEGDMA 550/HEMA system with the 8:2wt. ratio showed a more uniform increase in the storage modulus over the wavelength range. Under these conditions, the photoinitiator system was more compatible with the wavelengths. In addition, the final values of the storage modulus are higher than for the 1:1wt. ratio, probably because of the increased PEGDMA 550 content, which improves the network formation and rigidity of the material.

These results highlight the following two major points. First, the curing efficacy is primarily affected by the monomer ratio, which signifies dose-dependent crosslinking, as a higher number (8:2wt.) of PEGDMA 550 leads to effective crosslinking at either wavelength. Second, the photon energy is also important in curing. The shorter the wavelength, the more effective the polymerization. Moreover, in systems containing a higher amount of PEGDMA 550, the curing process appears to be less wavelength dependent.

The shrinkage results provide insight into how the monomer systems behave during photopolymerization at different wavelengths (Fig. 12). The PEGDMA 550/HEMA system with a 1:1wt. ratio started with the greatest shrinkage at 565 nm (0.8%) and 660 nm (0.7%). In addition, a more significant polymerization led to greater shrinkage. The least shrinkage occurred at 530 nm and 595 nm (0.1%), confirming the reduced efficiency of polymerization. At 405 nm, the shrinkage was moderate (0.5%), which suggests a comprehensive polymerization process that necessitates further contraction. In addition, the contraction depended on the intensity of the diode radiation. The higher the intensity emitted by a given diode, the greater the shrinkage of the irradiated composition. The diode at 565nm had the highest intensity at 34.68 mW/cm^2.

On the other hand, the PEGDMA550/HEMA system at an 8:2wt. ratio revealed that the maximum shrinkage was at 565 nm, which is 1%, and 405 and 660 nm have similar shrinkages of 0.8%. Shrinkage at 530 nm was the lowest (0.4%). The 8:2wt. system had a higher level of shrinkage than the 1:1wt. ratio because of the increased amount of PEGDMA 550, which had a packing effect.

According to the present findings, the monomer ratio and light wavelength influence the shrinkage. In both formulations, the maximum shrinkage was observed at 565 nm, which is thought to be associated with the peak absorption of the photoinitiator system at peak efficiency. When the PEGDMA 550 content is higher, when the ratio is 8:2wt., shrinkage is enhanced for all wavelengths due to its higher crosslinking potential and more significant polymerization contraction.

This research highlights some crucial photopolymerization behavior trends in PEGDMA 550/HEMA systems. First, lower wavelengths (ex., 405 nm) effectively and rapidly begin the curing process. As a result, the storage modulus was very high. Nonetheless, according to the composition of the monomers and the photoinitiator system, even longer wavelengths (e.g., 565 nm and 660 nm) may achieve curing efficiency. Second, the curing efficiency was enhanced by a higher storage modulus (preventing the increase in PEGDMA 550 content to an 8:2wt. ratio). Furthermore, the bio-inclusion process was more homogeneous across wavelengths. However, this also results in more material shrinkage, which may be a drawback for applications with dimensional requirements. The photoinitiator (BLUE/MDEA/Speedcure 938) ultimately depends on the monomer composition and wavelength of light. The wavelength and monomer ratio should be optimized for practical applications to ensure proper curing without shrinkage.

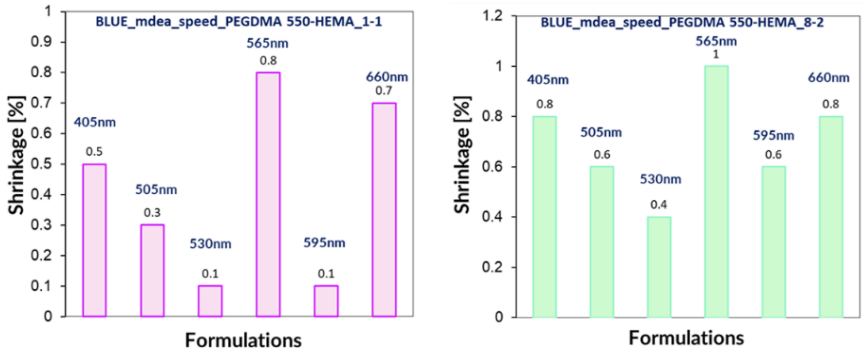

Wavelength (nm)	Intensity (mW/cm^2)
@405	22.79
@505	17.23
@530	12.11
@565	34.68
@595	13.22
@660	26.34

(c)

Figure 12. Comparison of the shrinkage of the photoinitiating systems based on Blue (0.1wt.%), Speedcure 938(1.0wt.%) and MDEA (1.5wt.%), film thickness 100 μm. a) PEGDMA 550:HEMA ratio 1:1, b) PEGDMA 550:HEMA ratio 8:2wt. c) intensity of used sources of light.

According to this study, the formulation of light-curable products can be tailored towards specific applications. The desired mechanical and dimensional stability performance of the final material can be achieved by changing the wavelengths and the number of monomers.

3.5. Development of hydrogel polymer materials

To test the properties of the hydrogels, the developed materials with thicknesses of 1, 1.5, and 2 mm were weighed and immersed in water (Table 4). After 24 h, the hydrogels were removed, weighed, and placed with a sponge in the solution; the operation was repeated after 48h. The weight of the hydrogel materials increased owing to water absorption. water absorption was almost 100% for the 2 mm thick hydrogel. The materials were shelf-stable, and water was retained in their structures. This demonstrates the ability of the developed materials to absorb water, which opens up various possibilities for their application as active ingredients in care and treatment products.

3.6. Three-dimensional printing of the hydrogel model structure

Figure 13 presents the experimental results of the 3D printing of hydrogels at different concentrations of photoinitiator compositions and setups. This study aimed to determine how the photoinitiator concentrations in printer inks affect the quality, resolution, and architecture of 3D-DLP hydrogel constructs. The materials were durable and water was effectively retained within their structures, demonstrating their capacity for water absorption. This property offers various opportunities for use as active components in cosmetic and therapeutic products. At the same time, regarding potential applications in medical devices, safety and biocompatibility issues need to be considered. The manuscript now discusses relevant literature on the toxicity of similar materials and highlights the need for future studies to fully assess safety before any medical application. The printed hydrogels were based on compositions containing varying concentrations

Table 4. Weight changes of hydrogels incubated in water for 48 h.

Hydrogel thickness	Initial weight [mg]	Weight after 24h [mg]	Weight after 48h [mg]
1 × 1 × 1 mm	170	220	255
1 × 1 × 1.5 mm	300	395	476
1 × 1 × 2 mm	383	514	609

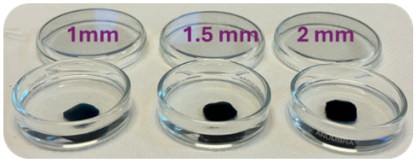

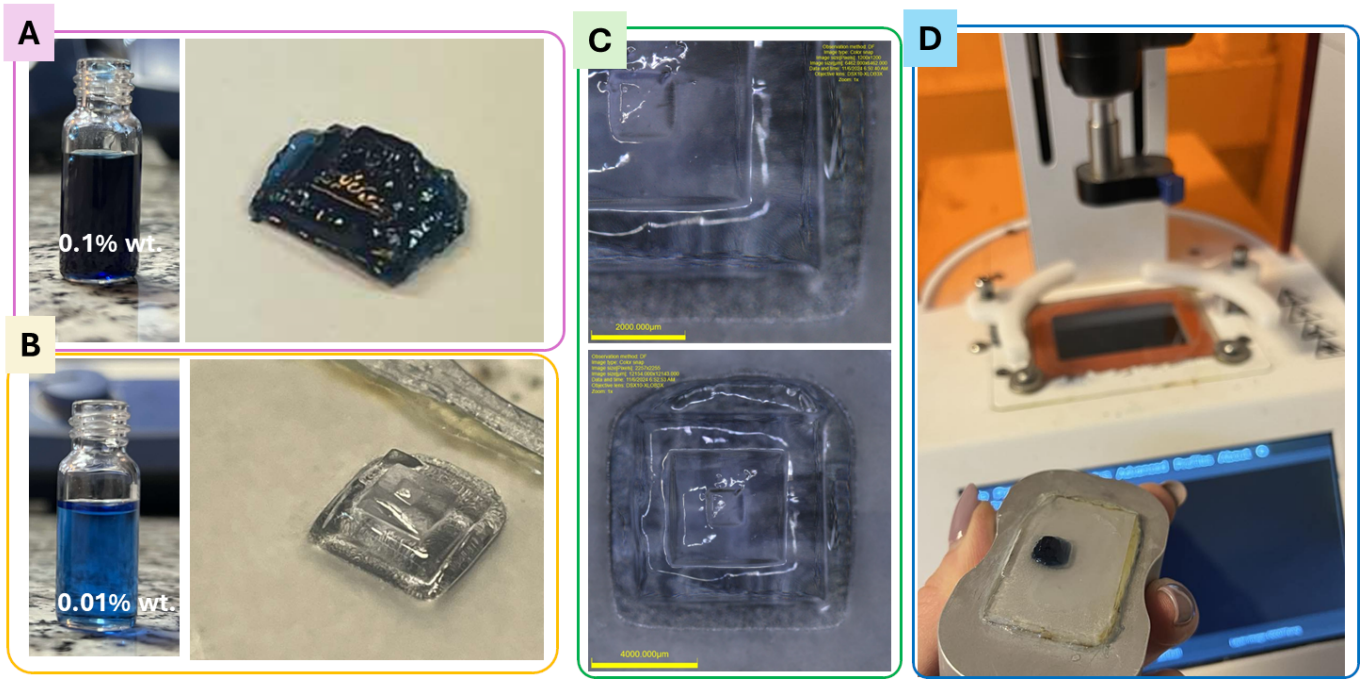

Figure 13. (A) Printing from a composition containing Blue (0.1% wt.), Speedcure 938 (1% wt.) and MDEA (3% wt.) in the presence of PEGDMA 550/HEMA 8/2 monomers (B) Printing from a composition containing Blue (0.01% wt.), Speedcure 938 (1% wt.) and MDEA(3% wt.) in the presence of PEGDMA 550/HEMA 8:2 monomers (C) printed 3D pattern in visible light on optical microscope DSX-HRSU from OLYMPUS Corporation (D) LUMEN X Gen 3, Cellink – the innovative printer used to obtain the printouts in this paper.

of a photoinitiator (DB1) combined with Speedcre938 and MDEA within a PEGDMA550/HEMA 8:2 monomer matrix (Fig. 13). Two distinct concentrations of the photoinitiator, 0.1% wt. (panel A) and 0.01% wt. (panel B) was used to assess the impact on printing quality. The experiments used an optical microscope setup (Panel C) and an advanced Lumen X Gen 3 bioprinter from Cellink (Panel D).

The experiments with a higher photoinitiator concentration (0.1% wt.) produced dark-colored hydrogels. The printed structures were well-formed but could not achieve finer details because, at high photoinitiator concentrations, excessive light absorption and limited penetration depth inhibited proper polymerization reactions. Conversely, the concentration of photoinitiator of 0.01% wt. in the formulations produced lighter colored hydrogels because of their lower photopolymerization efficiencies. The lowest concentrations of the final structures displayed a superior translucency and finer resolution. The printed hydrogel structures were viewed under a microscope to determine the surface smoothness and resolution of dishes or samples. Printed structures with a 0.01% wt. concentration had sharper edges and finer details, proving that printing accuracy was achievable at low photoinitiator concentrations.

According to these results, the concentration of the photoinitiator significantly affected the quality of the hydrogel constructs. A higher concentration of 0.1% weight ensures polymerization although the resolution and details will suffer when the concentration of the component is reduced to 0.01% wt. This helps to obtain finer details and better light penetration at the cost of optimized exposure times for better polymerization. Using advanced 3D bioprinting technology, this study aimed to construct precisely designed structures to optimize the printing process for biomedical applications, such as tissue engineering and drug delivery systems. Currently, this technology enables the creation of complex tissue structures, including tumor models for studying interactions between healthy and diseased cells (Awuah et al., 2025) and the precise design of artificial blood vessels, which is crucial for producing functional tissues and organs (Dong et al., 2024; Sexton et al., 2023).

It should be emphasized that our materials require comprehensive studies on toxicity, cytotoxicity, and biocompatibility before they can be applied in medical products. This represents an important direction for future research, which will determine their potential use in tissue engineering and drug delivery systems.

4. CONCLUSIONS

These findings underscore the potential of DB1 dye for advancing photopolymerization technologies. Beyond its primary role as a photosensitizer, the dye's robust photochemical and luminescent properties make it a cornerstone for the development of next-generation materials. Studies on related organic dyes and photosensitizers have demonstrated that such compounds not only enhance the reaction kinetics but also enable the synthesis of highly functionalized polymeric materials with tailored properties, such as improved mechanical strength, thermal stability, and biocompatibility. In conclusion, comprehensive research on the properties and applications of DB1 highlights its role as a key ingredient in photopolymerization. Its integration with light-based manufacturing and functional material development reflects a growing focus on sustainability, efficiency, and innovation. Future research should focus on optimizing their use in hybrid systems, expanding their range of applications, and exploring synergies with other advanced photoinitiators to fully unlock their potential.

ACKNOWLEDGEMENTS

*The research was funded by the **National Science Centre** (NCN, Poland) from the science budget between 2022 and 2026 as a research project within the **'OPUS'** program project no: UMO-2021/41/B/ST5/04533.*

*Thanks are also due to the **Ministry of Science and Higher Education** for funding the research within the **'Pearls of Science'** competition 'Initiating systems for printing hydrogels with controlled conductivity and mechanical properties'; project no: PN/01/0042/2022.*

REFERENCES

Al Rashid A., Ahmed W., Khalid M.Y., Koç M., 2021. Vat photopolymerization of polymers and polymer composites: processes and applications. *Addit. Manuf.*, 47, 102279. DOI: 10.1016/j.addma.2021.102279.

Anselmo A.C., Mitragotri S., 2014. An overview of clinical and commercial impact of drug delivery systems. *J. Controlled Release*, 190, 15–28. DOI: 10.1016/j.jconrel.2014.03.053.

Awuah W.A., Karkhanis S., Ben-Jaafar A., Kong J.S.H., Mannan K.M., Nkrumah-Boateng P.A., Tan J.K., Dorcas A.O., Shet V., Shah M.H., Abdul-Rahman T., Atallah O., 2025. Recent advances in 3D printing applications for CNS tumours. *Eur. J. Med. Res.*, 30, 251. DOI: 10.1186/s40001-025-02483-w.

Bagheri A., Jin J., 2019. Photopolymerization in 3D Printing. *ACS Appl. Polym. Mater.*, 1, 593–611. DOI: 10.1021/acsapm.8b00165.

Bao Y., 2022. Recent trends in advanced photoinitiators for vat photopolymerization 3D printing. *Macromol. Rapid Commun.*, 43, 2200202. DOI: 10.1002/marc.202200202.

Baryshnikov G., Minaev B., Ågren H., 2017. Theory and calculation of the phosphorescence phenomenon. DOI: 10.1021/acs.chemrev.7b00060.

Chimene D., Lennox K.K., Kaunas R.R., Gaharwar A.K., 2016. Advanced bioinks for 3D printing: a materials science perspective. *Ann. Biomed. Eng.*, 44, 2090–2102. DOI: 10.1007/s10439-016-1638-y.

Crivello J.V., Reichmanis E., 2014. Photopolymer materials and processes for advanced technologies. *Chem. Mater.*, 26, 533–548. DOI: 10.1021/cm402262g.

Currens E.R., Armbruster M.R., Castiaux A.D., Edwards J.L., Martin R.S., 2022. Evaluation and optimization of PolyJet 3D printed materials for cell culture studies. *Anal. Bioanal. Chem.*, 414, 3329–3339. DOI: 10.1007/s00216-022-03991-y.

Decker C., Bianchi C., Decker D., Morel F., 2001. Photoinitiated polymerization of vinyl ether-based systems. *Prog. Org. Coat.*, 42, 253–266. DOI: 10.1016/S0300-9440(01)00203-X.

Dissanayake W., Zadeh H.N., Nazmi A.R., Stevens C., Huber T., Abhayawardhana P.L., 2024. Exploring the potential of 3D-printable agar–urea hydrogels as an efficient method of delivering nitrogen in agricultural applications. *Polysaccharides,* 5, 49–66. DOI: 10.3390/polysaccharides5010004.

Distler T., Boccaccini A.R., 2020. 3D printing of electrically conductive hydrogels for tissue engineering and biosensors – a review. *Acta Biomater.*, 101, 1–13. DOI: 10.1016/j.actbio.2019.08.044.

do Nascimento G.M., de Oliveira R.C., Pradie N.A., Lins P.R.G., Worfel P.R., Martinez G.R., Di Mascio P., Dresselhaus M.S., Corio P., 2010. Single-wall carbon nanotubes modified with organic dyes: synthesis, characterization and potential cytotoxic effects. *J. Photochem. Photobiol. A: Chem.*, 211, 99–107. DOI: 10.1016/j.jphotochem.2010.01.019.

Dong C., Petrovic M., Davies I.J., 2024. Applications of 3D printing in medicine: a review. *Ann. 3D Print. Med.*, 14, 100149. DOI: 10.1016/j.stlm.2024.100149.

Drury J.L., Mooney D.J., 2003. Hydrogels for tissue engineering: scaffold design variables and applications. *Biomater.*, 24, 4337–4351. DOI: 10.1016/S0142-9612(03)00340-5.

El-Rehim H.A.A., Hegazy E.-S.A., El-Mohdy H.L.A., 2004. Radiation synthesis of hydrogels to enhance sandy soils water retention and increase plant performance. *J. Appl. Polym. Sci.*, 93, 1360–1371. DOI: 10.1002/app.20571.

Fertier L., Koleilat H., Stemmelen M., Giani O., Joly-Duhamel C., Lapinte V., Robin J.-J., 2013. The use of renewable feedstock in UV-curable materials – a new age for polymers and green chemistry. *Prog. Polym. Sci.*, 38, 932–962. DOI: 10.1016/j.progpolymsci.2012.12.002.

Fiedor P., Pilch M., Szymaszek P., Chachaj-Brekiesz A., Galek M., Ortyl J., 2020. Photochemical study of a new bimolecular photoinitiating system for vat photopolymerization 3D printing techniques under visible light. *Catalysts*, 10, 284–304. DOI: 10.3390/catal10030284.

Garino S., Antonaci P., Pastrone D., Sangermano M., Maggi F., 2021. Photo-polymerization for additive manufacturing of composite solid propellants. *Acta Astronaut.*, 182, 58–65. DOI: 10.1016/j.actaastro.2021.01.062.

Gibson I., Rosen D., Stucker B., 2015. *Additive manufacturing technologies: 3D printing, rapid prototyping, and direct digital manufacturing*. 2nd edition, Springer, New York. DOI: 10.1007/978-1-4939-2113-3.

Gulrajani M.L., 2011. 10 – Disperse dyes, In: Clark M. (Ed.), *Handbook of textile and industrial dyeing*, Vol. 1: Principles, processes and types of dyes. Woodhead Publishing Limited, 365-394. DOI: 10.1533/9780857093974.2.365.

Hola E., Fiedor P., Dzienia A., Ortyl J., 2021. Visible-light amine thioxanthone derivatives as photoredox catalysts for photopolymerization processes. *ACS Appl. Polym. Mater.,* 3, 5547–5558. DOI: 10.1021/acsapm.1c00886.

Hola E., Pilch M., Ortyl J., 2020. Thioxanthone derivatives as a new class of organic photocatalysts for photopolymerisation processes and the 3D printing of photocurable resins under visible light. *Catalysts*, 10, 903. DOI: 10.3390/catal10080903.

Hou J., Dong J., Zhu H., Teng X., Ai S., Mang M., 2015. A simple and sensitive fluorescent sensor for methyl parathion based on L-tyrosine methyl ester functionalized carbon dots. *Biosens. Bioelectron.*, 68, 20–26. DOI: 10.1016/j.bios.2014.12.037.

Jasinski F., Zetterlund P.B., Braun A.M., Chemtob A., 2018. Photopolymerization in dispersed systems. *Prog. Polym. Sci.*, 84, 47–88. DOI: 10.1016/j.progpolymsci.2018.06.006.

Kabatc J., Ortyl J., Kostrzewska K., 2017. New kinetic and mechanistic aspects of photosensitization of iodonium salts in photopolymerization of acrylates. *RSC Adv.*, 7, 41619–41629. DOI: 10.1039/c7ra05978g.

Kalossaka L.M., Sena G., Barter L.M.C., Myant C., 2021. Review: 3D printing hydrogels for the fabrication of soilless cultivation substrates. *Appl. Mater. Today*, 24, 101088. DOI: 10.1016/j.apmt.2021.101088.

Kamińska I., Ortyl J., Popielarz R., 2015. Applicability of quinolizino-coumarins for monitoring free radical photopolymerization by fluorescence spectroscopy. *Polym. Test.*, 42, 99–107. DOI: 10.1016/j.polymertesting.2014.12.013.

Kasprzyk W., Świergosz T., Bednarz S., Walas K., Bashmakova N.V., Bogdał D., 2018. Luminescence phenomena of carbon dots derived from citric acid and urea – a molecular insight. *Nanoscale*, 10, 13889–13894. DOI: 10.1039/c8nr03602k.

Khadilkar A., Wang J., Rai R., 2019. Deep learning-based stress prediction for bottom-up SLA 3D printing process. *Int. J. Adv. Manuf. Technol.*, 102, 2555–2569. DOI: 10.1007/s00170-019-03363-4.

Larush L., Kaner I., Fluksman A., Tamsut A., Pawar A.A., Lesnovski P., Benny O., Magdassi S., 2017. 3D printing of responsive hydrogels for drug-delivery systems. *J. 3D Print. Med.*, 1, 219–229. DOI: 10.2217/3dp-2017-0009.

Le C.M.Q., Petitory T., Wu X., Spangenberg A., Ortyl J., Galek M., Infante L., Thérien-Aubin H., Chemtob A., 2021. Water-soluble photoinitiators from dimethylamino-substituted monoacylphosphine oxide for hydrogel and latex preparation. *Macromol. Chem. Phys.*, 222, 2100217. DOI: 10.1002/macp.202100217.

Li J., Wu C., Chu P.K., Gelinsky M., 2020. 3D printing of hydrogels: rational design strategies and emerging biomedical applications. *Mater. Sci. Eng.: R: Rep.*, 140, 100543. DOI: 10.1016/j.mser.2020.100543.

Lin J.-T., Lalevee J., Cheng D.-C., 2021. A critical review for synergic kinetics and strategies for enhanced photopolymerizations for 3D-printing and additive manufacturing. *Polymers*, 13, 2325. DOI: 10.3390/polym13142325.

Liu C., Xu N., Zong Q., Yu J., Zhang P., 2021. Hydrogel prepared by 3D printing technology and its applications in the medical field. *Colloids Interface Sci. Commun.*, 44, 100498. DOI: 10.1016/j.colcom.2021.100498.

Ma S., Yu B., Pei X., Zhou F., 2016. Structural hydrogels. *Polymer*, 98, 516–535. DOI: 10.1016/j.polymer.2016.06.053.

Nowak D., Ortyl J., Kamińska-Borek I., Kukuła K., Topa M., Popielarz R., 2018. Photopolymerization of hybrid monomers, Part II: Determination of relative quantum efficiency of selected photoinitiators in cationic and free-radical polymerization of hybrid monomers. *Polym. Test.*, 67, 144–150. DOI: 10.1016/j.polymertesting.2018.02.025.

Ortyl J., Galek M., Milart P., Popielarz R., 2012. Aminophthalimide probes for monitoring of cationic photopolymerization by fluorescence probe technology and their effect on the polymerization kinetics. *Polym. Test.*, 31, 466–473. DOI: 10.1016/j.polymertesting.2012.01.008.

Ortyl J., Milart P., Popielarz R., 2013. Applicability of aminophthalimide probes for monitoring and acceleration of cationic photopolymerization of epoxides. *Polym. Test.*, 32, 708–715. DOI: 10.1016/j.polymertesting.2013.03.009.

Ortyl J., Topa M., Kamińska-Borek I., Popielarz R., 2019. Mechanism of interaction of aminocoumarins with reaction medium during cationic photopolymerization of triethylene glycol divinyl ether. *Eur. Polym. J.*, 116, 45–55. DOI: 10.1016/j.eurpolymj.2019.03.060.

Peer G., Eibel A., Gorsche C., Catel Y., Gescheidt G., Moszner N., Liska R., 2019. Ester-activated vinyl ethers as chain transfer agents in radical photopolymerization of methacrylates. *Macromolecules*, 52, 2691–2700. DOI: 10.1021/acs.macromol.9b00085.

Petko F., Galek M., Hola E., Popielarz R., Ortyl J., 2021. One-component cationic photoinitiators from tunable benzylidene scaffolds for 3D printing applications. *Macromolecules*, 54, 7070–7087. DOI:10.1021/acs.macromol.1c01048.

Petko F., Galek M., Hola E., Topa-Skwarczyńska M., Tomal W., Jankowska M., Pilch M., Popielarz R., Graff B., Morlet-Savary F., Lalevee J., Ortyl J., 2022. Symmetric iodonium salts based on benzylidene as one-component photoinitiators for applications in 3D printing. *Chem. Mater.*, 34, 10077–10092. DOI: 10.1021/acs.chemmater.2c02796.

Piedra-Cascón W., Krishnamurthy V.R., Att W., Revilla-León M., 2021. 3D printing parameters, supporting structures, slicing, and post-processing procedures of vat-polymerization additive manufacturing technologies: A narrative review. *J. Dent.*, 109, 103630. DOI: 10.1016/j.jdent.2021.103630.

Price R.B., Ferracane J.L., Hickel R., Sullivan B., 2020. The light-curing unit: an essential piece of dental equipment. *Int. Dent. J.,* 70, 407–417. DOI: 10.1111/idj.12582.

Qu S., Wang X., Lu Q., Liu X., Wang L., 2012. A biocompatible fluorescent ink based on water-soluble luminescent carbon nanodots. *Angew. Chem. Int. Ed.*, 51, 12215–12218. DOI: 10.1002/anie.201206791.

Sanchez-Rexach E., Johnston T.G., Jehanno C., Sardon H., Nelson A., 2020. Sustainable materials and chemical processes for additive manufacturing. *Chem. Mater.,* 32, 7105–7119. DOI: 10.1021/acs.chemmater.0c02008.

Saquib M., Abu Tariq M., Haque M.M., Muneer M., 2008. Photocatalytic degradation of Disperse Blue 1 using $UV/TiO_2/H_2O_2$ process. *J. Environ. Manage.*, 88, 300–306. DOI: 10.1016/j.jenvman.2007.03.012.

Schmidt B.V.K.J., 2019. Hydrophilic polymers. *Polymers,* 11, 693. DOI: 10.3390/polym11040693.

Scott T.F., Cook W.D., Forsythe J.S., Bowman C.N., Berchtold K.A., 2003. FTIR and ESR spectroscopic studies of the photopolymerization of vinyl ester resins. *Macromolecules*, 36, 6066–6074. DOI: 10.1021/ma0259721.

Sexton Z.A., Hudson A.R., Herrmann J.E., Shiwarski D.J., Pham J., Szafron J.M., Wu S.M., Skylar-Scott M., Feinberg A.W., Marsden A., 2023. Rapid model-guided design of organ-scale synthetic vasculature for biomanufacturing. *arXiv*, arXiv:2308.07586. DOI: 10.48550/arXiv.2308.07586

Sun K., Zhang Y., Zhu D., Peng X., Zhang J., Gong T., Ma M., Xiao P., 2023. Visible-light photopolymerization activated by nanocarbon materials as photocatalysts. *J. Photochem. Photobiol., C: Photochem. Rev.*, 57, 100637. DOI: 10.1016/j.jphotochemrev.2023.100637.

Tasdelen M.A., Lalevée J., Yagci Y., 2020. Photoinduced free radical promoted cationic polymerization 40 years after its discovery. *Polym. Chem.*, 11, 1111–1121. DOI: 10.1039/c9py01903k.

Tehfe M.A., Louradour F., Lalevée J., Fouassier J.-P., 2013. Photopolymerization reactions: on the way to a green and sustainable chemistry. *Appl. Sci.*, 3, 490–514. DOI: 10.3390/app3020490.

Tomal W., Chachaj-Brekiesz A., Popielarz R., Ortyl J., 2020. Multifunctional biphenyl derivatives as photosensitisers in various types of photopolymerization processes, including IPN formation, 3D printing of photocurable multiwalled carbon nanotubes fluorescent composites. *RSC Adv.*, 10, 32162–32182. DOI: 10.1039/d0ra04146g.

Tomal W., Krok D., Chachaj-Brekiesz A., Lepcio P., Ortyl J., 2021a. Harnessing light to create functional, three-dimensional polymeric materials: multitasking initiation systems as the critical key to success. *Addit. Manuf.*, 48, 102447. DOI: 10.1016/j.addma.2021.102447.

Tomal W., Świergosz T., Pilch M., Kasprzyk W., Ortyl J., 2021b. New horizons for carbon dots: Quantum nano-photoinitiating catalysts for cationic photopolymerization and 3D printing under visible light. *Polym. Chem.*, 12, 3661–3676. DOI: 10.1039/d1py00228g.

Topa M., Petko F., Galek M., Ortyl J., 2020. Double role of diphenylpyridine derivatives as fluorescent sensors for monitoring photopolymerization and the determination of the efficiencies of the generation of superacids by cationic photoinitiators. *Sensors*, 20, 3043. DOI: 10.3390/s20113043.

Tran R.T., Yang J., Ameer G.A., 2015. Citrate-based biomaterials and their applications in regenerative engineering. *Annu. Rev. Mater. Res.*, 45, 277–310. DOI: 10.1146/annurev-matsci-070214-020815.

Tsegay F., Elsherif M., Butt H., 2022. Smart 3D printed hydrogel skin wound bandages: a review. *Polymers*, 14, 1012. DOI: 10.3390/polym14051012.

Valeur B., Berberan-Santos M.N., 2012. *Molecular Fluorescence: Principles and Applications*. 2nd ed., Wiley-VCH Verlag GmbH & Co. KGaA, Weinheim. DOI: 10.1002/9783527650002.

Wierzbicki S., Mielczarek K., Topa-Skwarczyńska M., Mokrzyński K., Ortyl J., Bednarz S., 2021. Visible light-induced photopolymerization of Deep Eutectic Monomers based on methacrylic acid and tetrabutylammonium salts with different anion structures. *Eur. Polym. J.*, 161, 110836. DOI: 10.1016/j.eurpolymj.2021.110836.

Williams D.F., 2008. On the mechanisms of biocompatibility. *Biomaterials*, 29, 2941–2953. DOI: 10.1016/j.biomaterials.2008.04.023.

Xiao P., Zhang J., Dumur F., Tehfe M.A., Morlet-Savary F., Graff B., Gigmes D., Fouassier J.P., Lalevée J., 2015. Visible light sensitive photoinitiating systems: Recent progress in cationic and radical photopolymerization reactions under soft conditions. *Prog. Polym. Sci.*, 41, 32–66. DOI: 10.1016/j.progpolymsci.2014.09.001.

You S., Wang P., Schimelman J., Hwang H.H., Chen S., 2019. High-fidelity 3D printing using flashing photopolymerization. *Addit. Manuf.*, 30, 100834. DOI: 10.1016/j.addma.2019.100834.

APPENDICES

A. Spectroscopic properties of Blue Disperse

A.1. Examples of steady state photolysis for Blue Disperse in acetonitrile

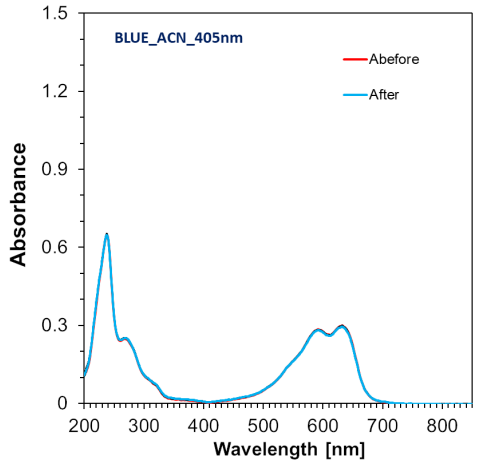

Figure A.1. Photolysis of Blue ACN under 405 nm, 400 mW.

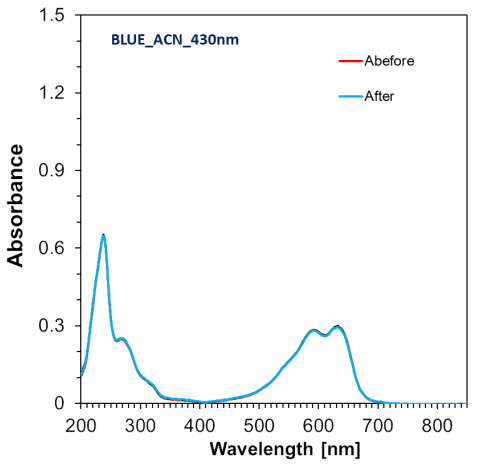

Figure A.2. Photolysis of Blue ACN under 430 nm, 400 mW.

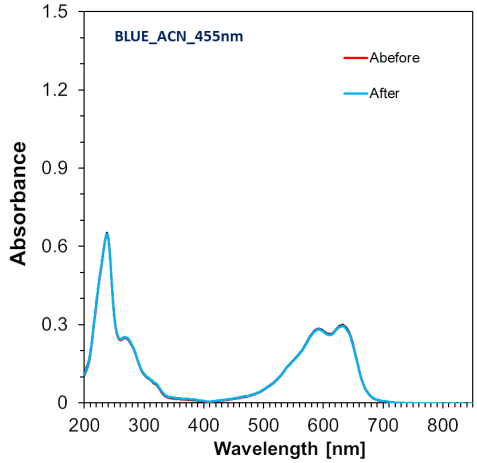

Figure A.3. Photolysis of Blue ACN under 455 nm, 400 mW.

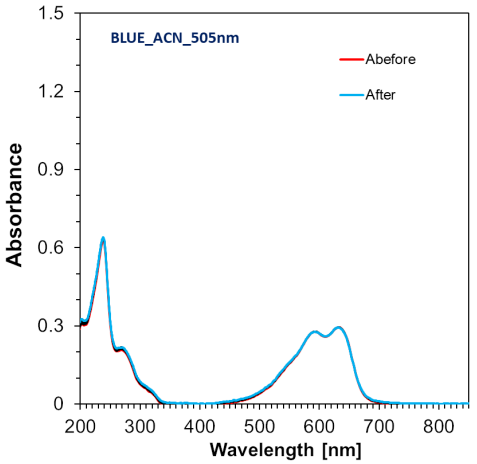

Figure A.4. Photolysis of Blue ACN under 505 nm, 400 mW.

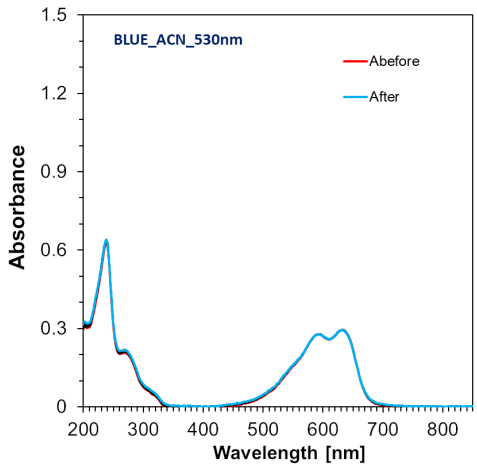

Figure A.5. Photolysis of Blue ACN under 530 nm, 400 mW.

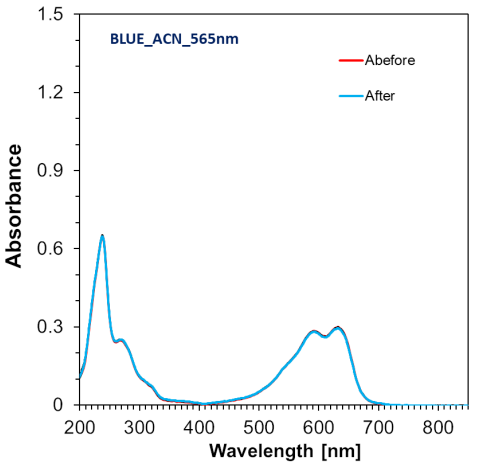

Figure A.6. Photolysis of Blue ACN under 565 nm, 400 mW.

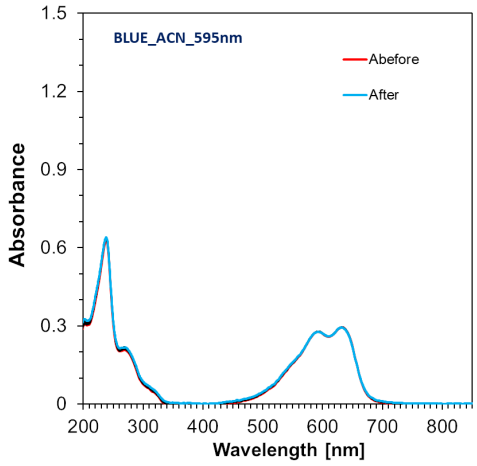

Figure A.7. Photolysis of Blue ACN under 595 nm, 400 mW.

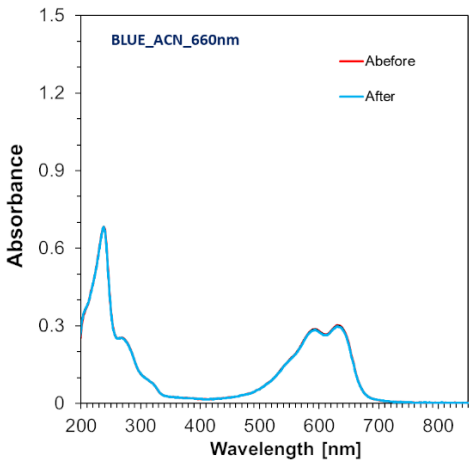

Figure A.8. Photolysis of Blue ACN under 660 nm, 400 mW.

A.2. Examples of steady state photolysis for Blue Disperse and with EDB in acetonitrile

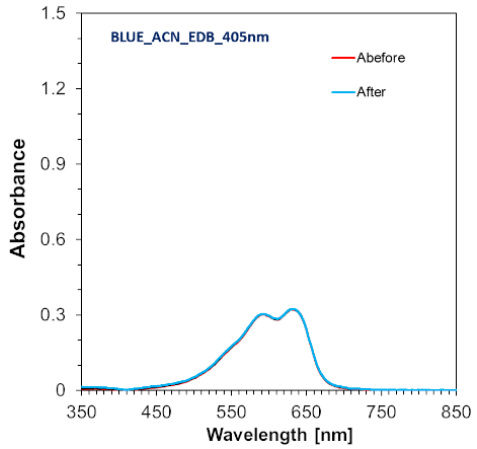

Figure A.9. Photolysis of Blue + EDB (concentration: $8.62{\cdot}10^{-3}$ [mol/dm^3]) in ACN under 405 nm, 400 mW.

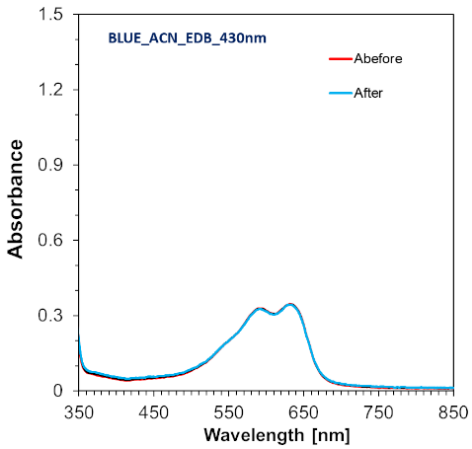

Figure A.10. Photolysis of Blue + EDB (concentration: $8.62{\cdot}10^{-3}$ [mol/dm^3]) in ACN under 430 nm, 400 mW.

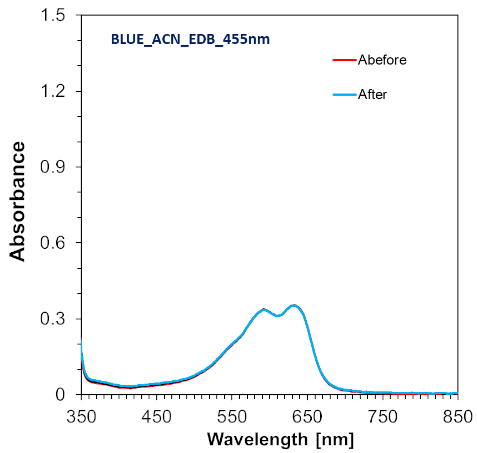

Figure A.11. Photolysis of Blue + EDB (concentration: $8.62{\cdot}10^{-3}$ [mol/dm^3]) in ACN under 455 nm, 400 mW.

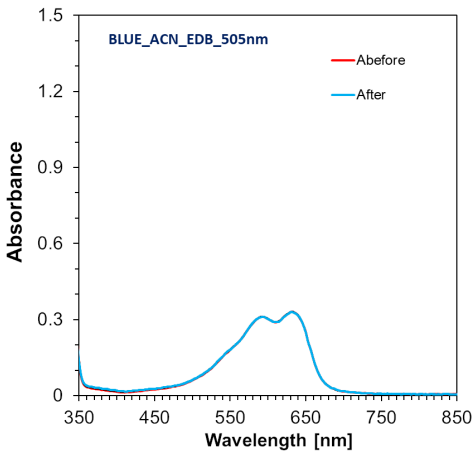

Figure A.12. Photolysis of Blue + EDB (concentration: $8.62{\cdot}10^{-3}$ [mol/dm^3]) in ACN under 505 nm, 400 mW.

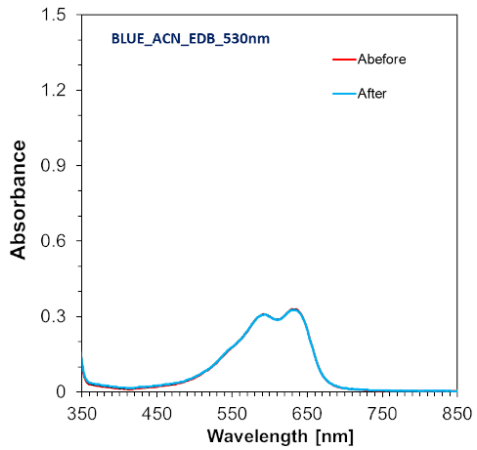

Figure A.13. Photolysis of Blue + EDB (concentration: $8.62 \cdot 10^{-3}$ [mol/dm^3]) in ACN under 530 nm, 400 mW.

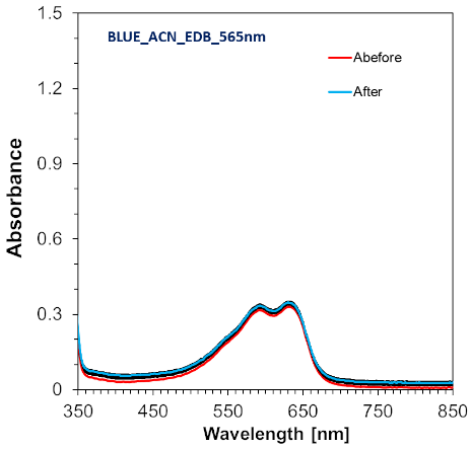

Figure A.14. Photolysis of Blue + EDB (concentration: $8.62 \cdot 10^{-3}$ [mol/dm^3]) in ACN under 565 nm, 400 mW.

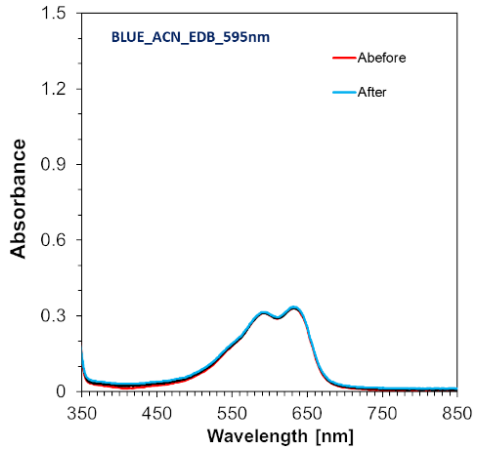

Figure A.15. Photolysis of Blue + EDB (concentration: $8.62 \cdot 10^{-3}$ [mol/dm^3]) in ACN under 595 nm, 400 mW.

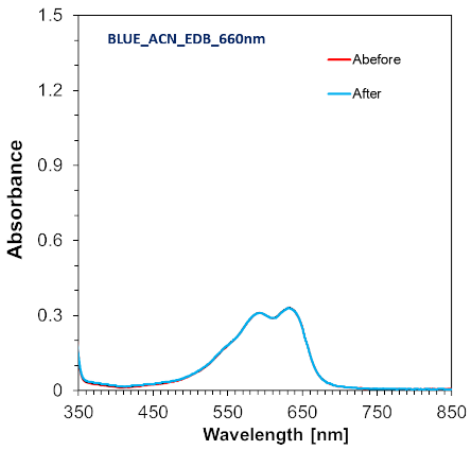

Figure A.16. Photolysis of Blue + EDB (concentration: $8.62 \cdot 10^{-3}$ [mol/dm^3]) in ACN under 660 nm, 400 mW.

A.3. Examples of steady state photolysis for Blue Disperse and with MDEA in acetonitrile

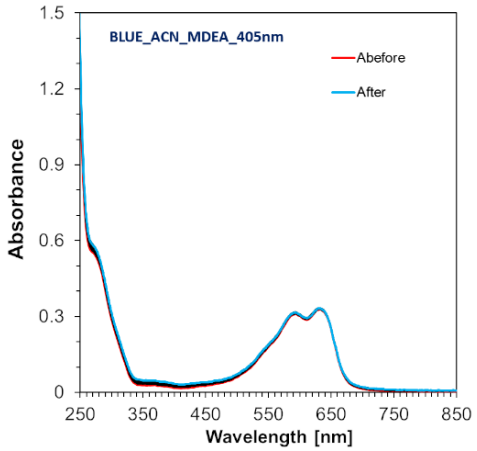

Figure A.17. Photolysis of Blue + MDEA (concentration: $13.9 \cdot 10^{-3}$ [mol/dm^3]) in ACN under 405 nm, 400 mW.

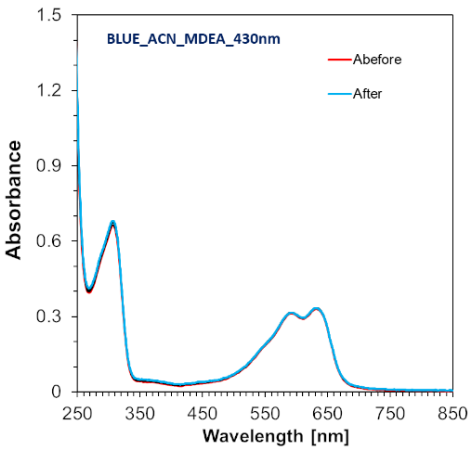

Figure A.18. Photolysis of Blue + MDEA (concentration: $13.9 \cdot 10^{-3}$ [mol/dm^3]) in ACN under 430 nm, 400 mW.

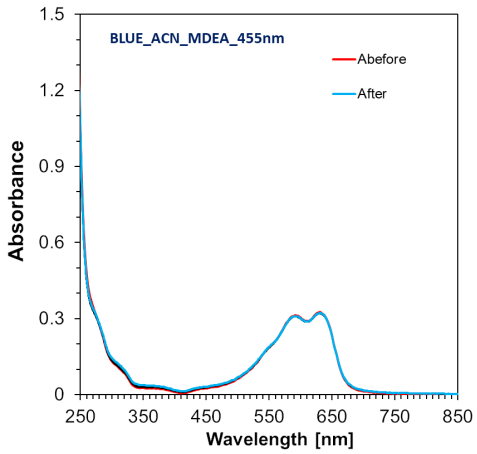

Figure A.19. Photolysis of Blue + MDEA (concentration: $13.9 \cdot 10^{-3}$ [mol/dm^3]) in ACN under 455 nm, 400 mW.

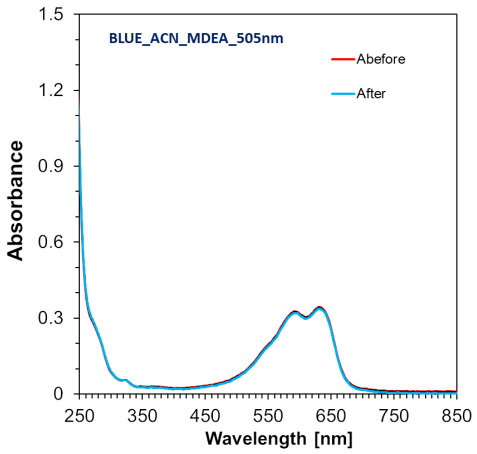

Figure A.20. Photolysis of Blue + MDEA (concentration: $13.9 \cdot 10^{-3}$ [mol/dm^3]) in ACN under 505 nm, 400 mW.

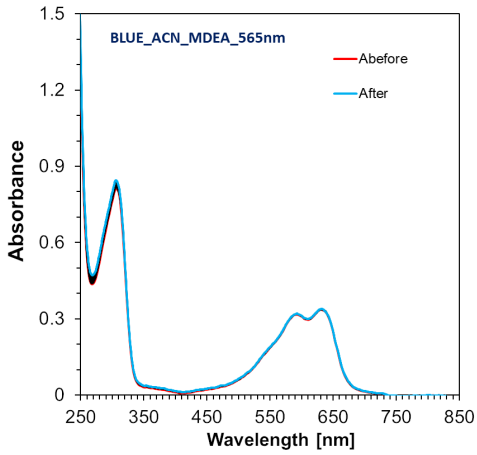

Figure A.21. Photolysis of Blue + MDEA (concentration: $13.9 \cdot 10^{-3}$ [mol/dm^3]) in ACN under 565 nm, 400 mW.

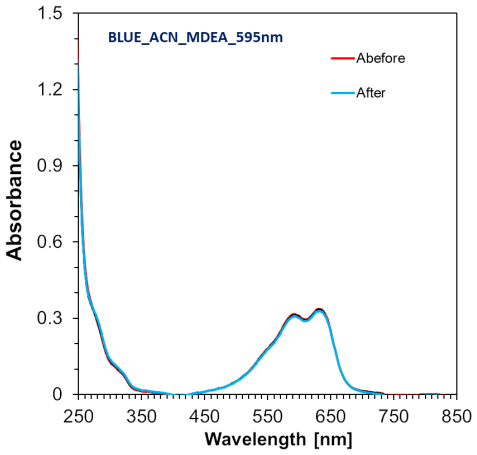

Figure A.22. Photolysis of Blue + MDEA (concentration: $13.9 \cdot 10^{-3}$ [mol/dm^3]) in ACN under 595 nm, 400 mW.

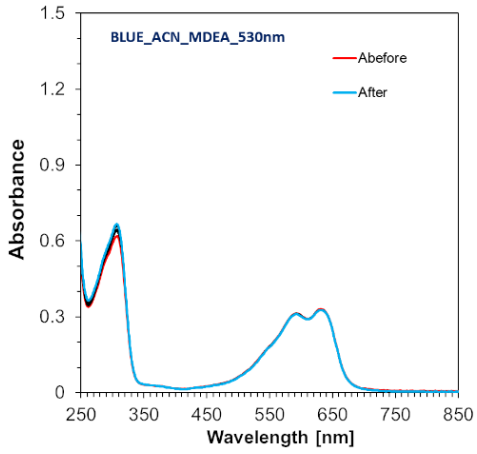

Figure A.23. Photolysis of Blue + MDEA (concentration: $13.9 \cdot 10^{-3}$ [mol/dm^3]) in ACN under 530 nm, 400 mW.

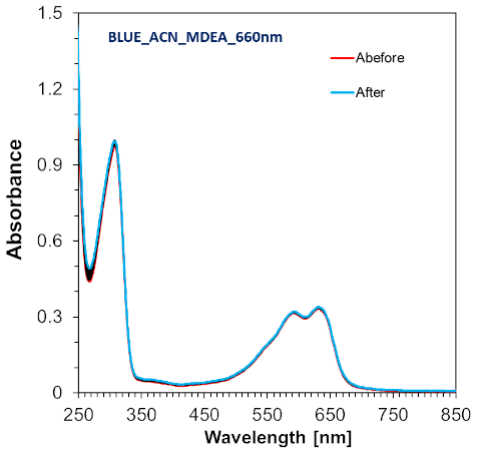

Figure A.24. Photolysis of Blue + MDEA (concentration: $13.9 \cdot 10^{-3}$ [mol/dm^3]) in ACN under 660 nm, 400 mW.

A.4. Examples of steady state photolysis for Blue Disperse and with Speedcure 938 in acetonitrile

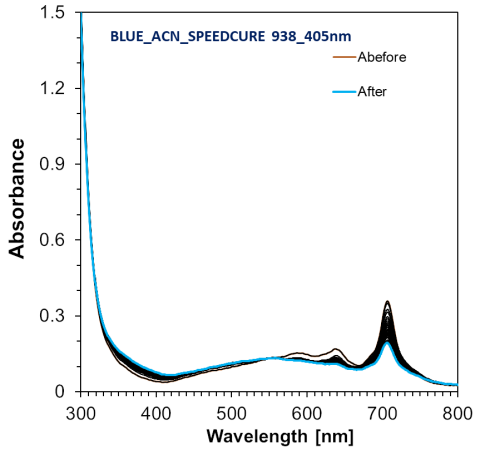

Figure A.25. Photolysis of Blue + Speedcure 938 (concentration: $3.09 \cdot 10^{-3}$ [mol/dm^3]) in ACN under 405 nm, 400 mW.

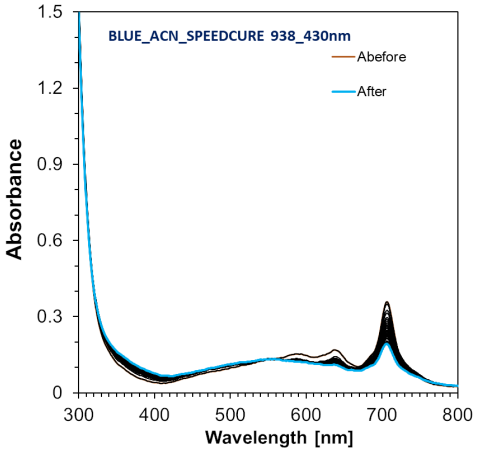

Figure A.26. Photolysis of Blue + Speedcure 938 (concentration: $3.09 \cdot 10^{-3}$ [mol/dm^3]) in ACN under 430 nm, 400 mW.

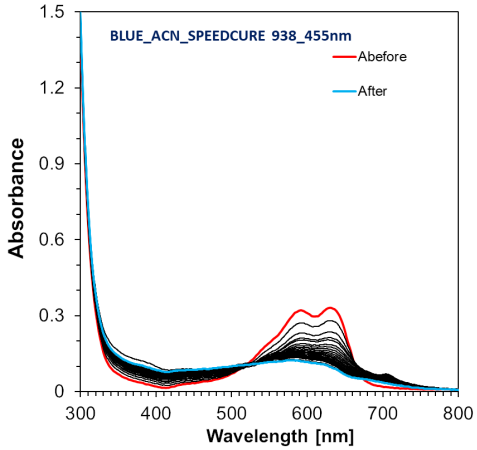

Figure A.27. Photolysis of Blue + Speedcure 938 (concentration: $3.09 \cdot 10^{-3}$ [mol/dm^3]) in ACN under 455 nm, 400 mW.

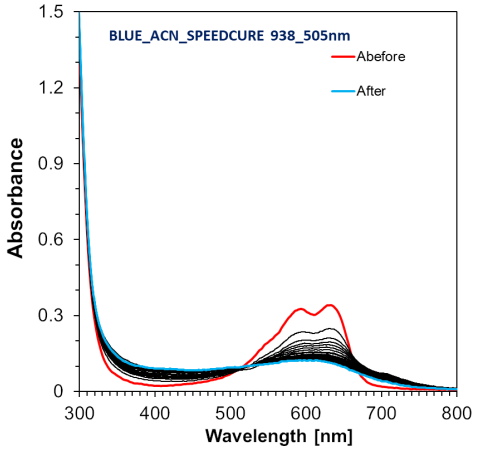

Figure A.28. Photolysis of Blue + Speedcure 938 (concentration: $3.09 \cdot 10^{-3}$ [mol/dm^3]) in ACN under 505 nm, 400 mW.

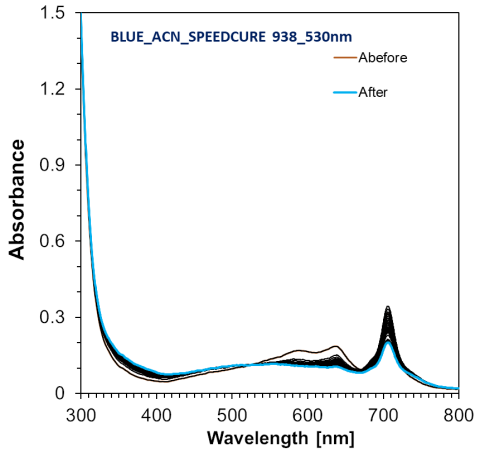

Figure A.29. Photolysis of Blue + Speedcure 938 (concentration: $3.09 \cdot 10^{-3}$ [mol/dm^3]) in ACN under 530 nm, 400 mW.

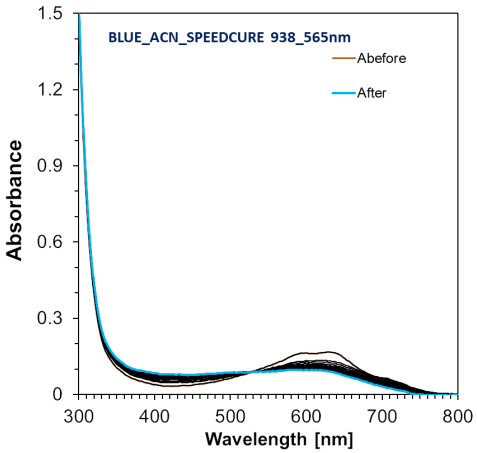

Figure A.30. Photolysis of Blue + Speedcure 938 (concentration: $3.09 \cdot 10^{-3}$ [mol/dm^3]) in ACN under 565 nm, 400 mW.

B. Electrochemical studies of co-initiator

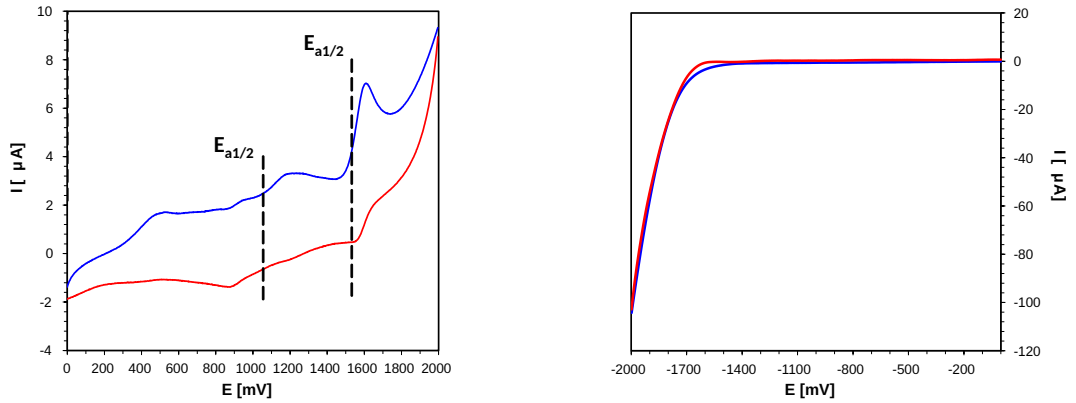

(a) Blue oxidation (b) Blue reduction

Figure B.1. Cyclic voltammogram in acetonitrile (with 0.1 M solution of tetrabutylammonium hexafluorophosphate electrolyte and Ag/AgCl as reference electrode, scan rate 100 mV/s) of the: (a) Blue oxidation, (b) Blue reduction.

C. Monitored band disappearance for the determination of conversion degrees in the Real-Time FT-IR method

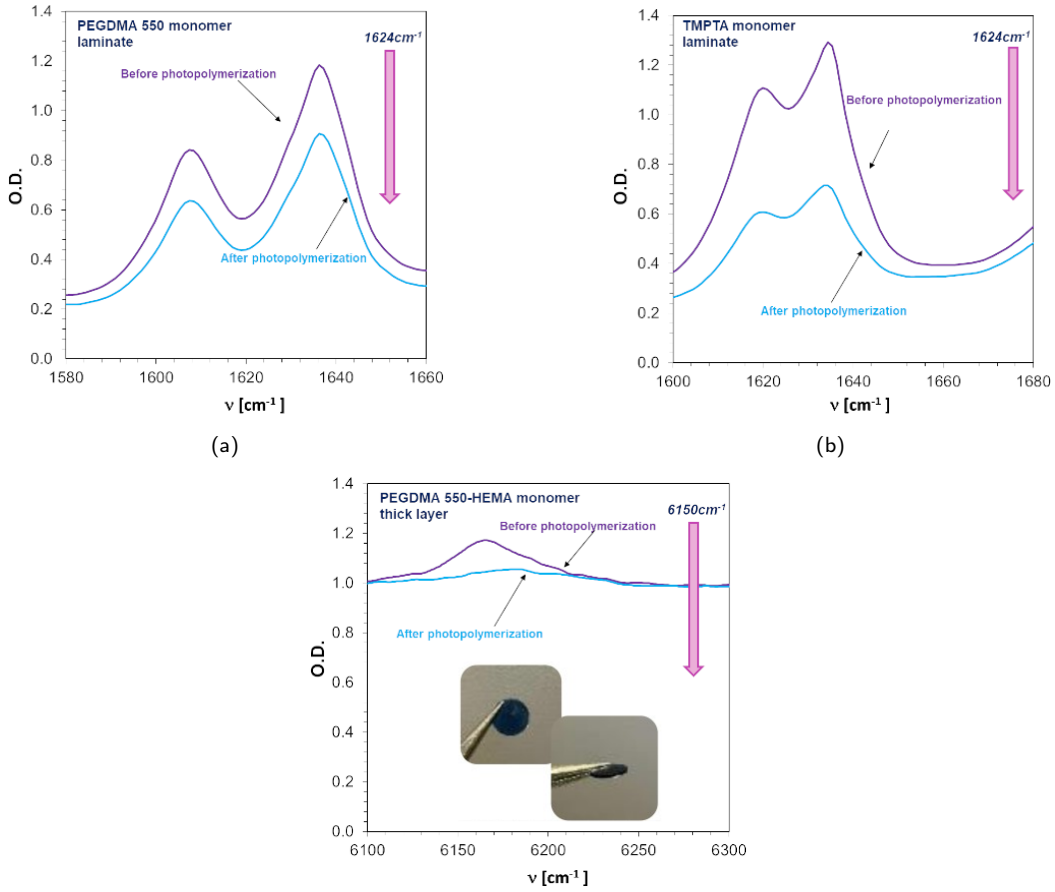

(a) (b)

(c)

Figure C.1. FT-IR spectra before and after photopolymerization a) monomer PEGDMA 550 in laminate (25 µm) under Vis-LED 405 nm irradiation, b) monomer TMPTA in laminate under Vis-LED 365 nm irradiation (25 µm), c) monomers PEGDMA550-HEMA in thick layer (1 mm) under Vis-LED 405 nm irradiation.

D. Parameters for polymeric coatings (1.0 mm) of samples composed of PEGDMA 550/HEMA and an initiator system in the form of Blue Disperse, MDEA and Speedcure 938

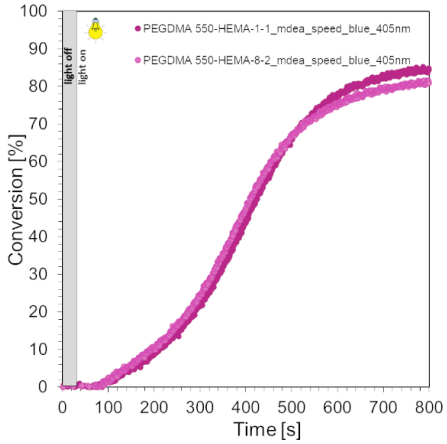

(a) LED@405 nm

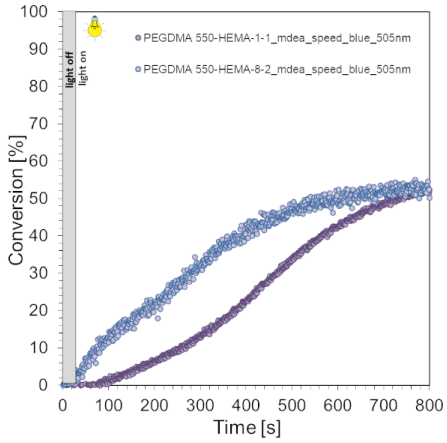

(b) LED@505 nm

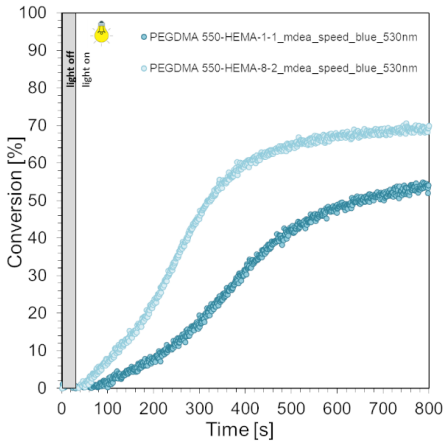

(c) LED@530 nm

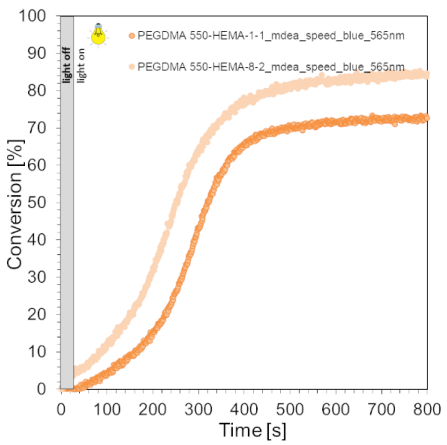

(d) LED@565 nm

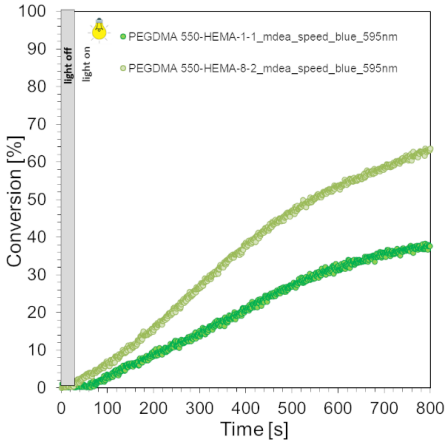

(e) LED@595 nm

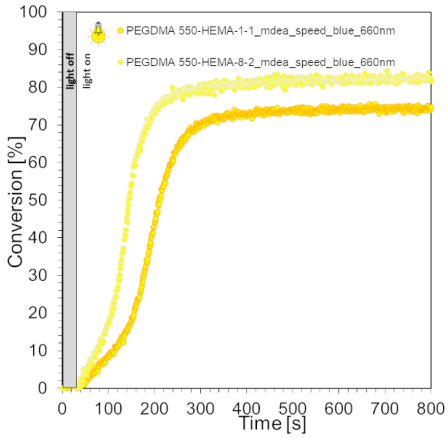

(f) LED@660 nm

Figure D.1. FT-IR spectra before and after photopolymerization of formulations composed of Blue (0.1% wt.), MDEA (1.5% wt.), IOD (1% wt.), and a mixture of PEGDMA 550/HEMA monomers (1/1); The thickness of the sample was 1mm upon exposure to the a) LED@405 nm, b) @505 nm, c) @530 nm, d) @565 nm, e) @590 nm, f) @660 nm. The irradiation starts at $t = 10$ s.

Table D.1. Coatings after radical photopolymerization of PEGDMA 550-HEMA monomers in thick layer (1 mm) and three-component initiating system Blue (0.1% w/w), IOD (1% w/w), MDEA (1.5% wt.).

Source of light	Formulations	
	Blue+MDEA+Speedcure 938 PEGDMA 550/HEMA 1/1	Blue+MDEA+Speedcure 938 PEGDMA 550-HEMA 8/2
LED @405		
LED @505		
LED @530		
LED @565		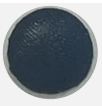
LED @595		
LED @660		

E. Polymerization shrinkage analysis and gel point

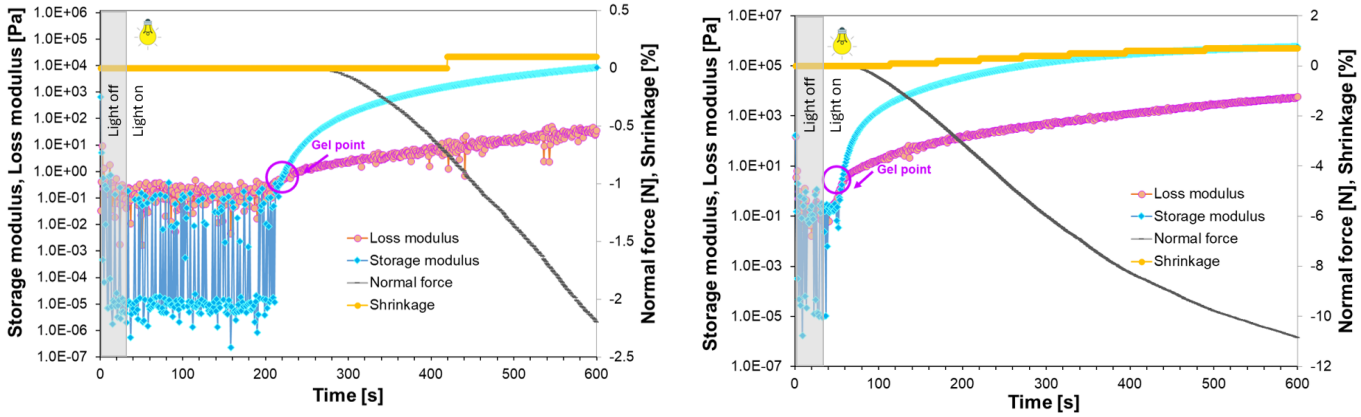

(a) (b)

Figure E.1. Storage modulus (blue), loss modulus (pink), normal force (black), shrinkage (yellow) as a function of irradiation time for the composition contain: (a) Blue (0.1% w/w), IOD (1% w/w), MDEA (1.5% wt.) and mixture PEGDMA 550/HEMA in weight ratio 1/1 under LED @505 nm irradiation.; (b) Blue (0.1% w/w), IOD (1% w/w), MDEA (1.5% wt.) and mixture PEGDMA 550/HEMA in weight ratio 8/2 under LED @505 nm irradiation.

F. Digital Microscope observation

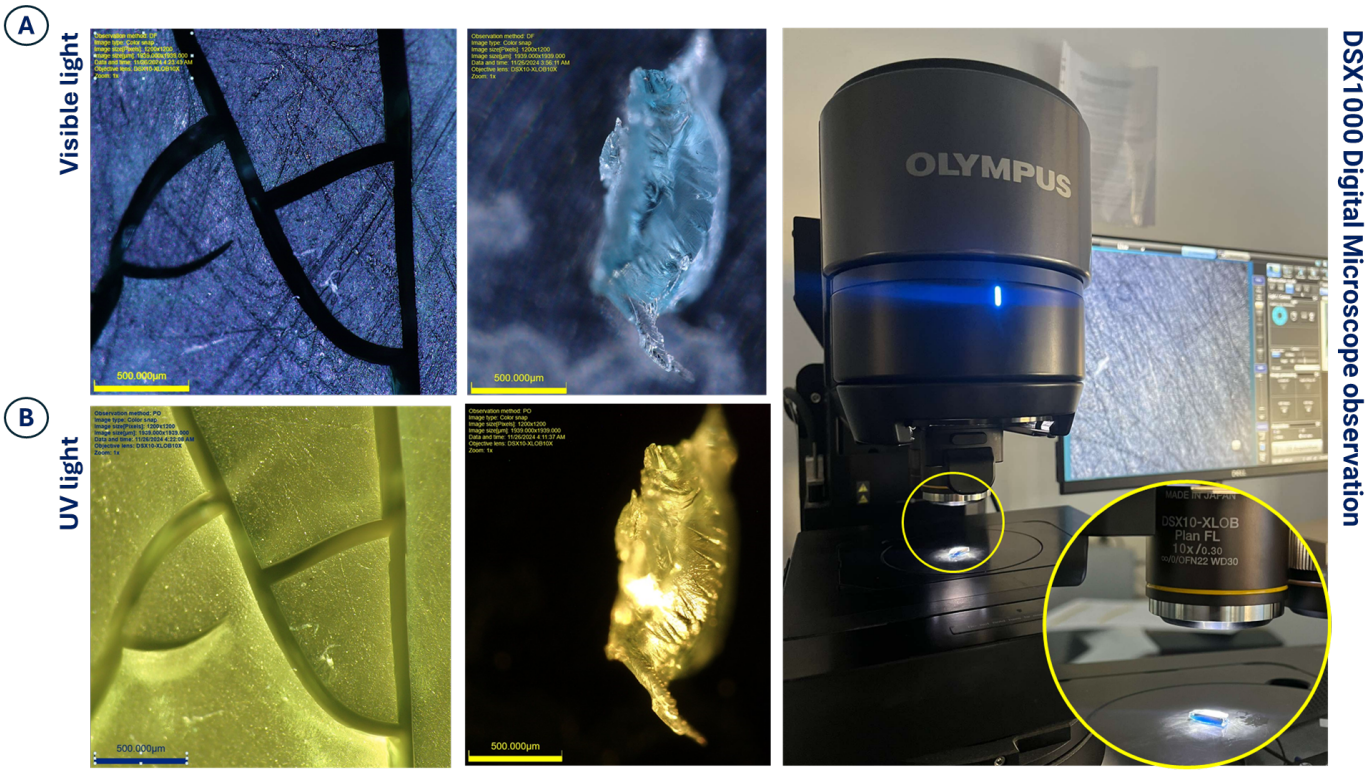

Figure F.1. Images of hydrogels after incubation in water observed under an Olympus digital microscope in (A) daylight and (B) under ultraviolet light.